Global Biogeochemical Cycles

RESEARCH ARTICLE
10.1029/2018GB005877

The Significance of Giant Phaeodarians (Rhizaria) to Biogenic Silica Export in the California Current Ecosystem

Tristan Biard[1], **Jeffrey W. Krause**[2,3], **Michael R. Stukel**[4], **and Mark D. Ohman**[1]

[1]Scripps Institution of Oceanography, University of California, San Diego, La Jolla, CA, USA, [2]Dauphin Island Sea Lab, Dauphin Island, AL, USA, [3]Department of Marine Sciences, University of South Alabama, Mobile, AL, USA, [4]Earth, Ocean, and Atmospheric Science Department, Florida State University, Tallahassee, FL, USA

Key Points:
- Phaeodarian skeletons contain large amounts of silica (0.37–43.42 μg Si/cell) that can be predicted from cell size and biovolume
- Phaeodarian contribution to $bSiO_2$ export from the euphotic zone increases substantially toward oligotrophic regions with low total $bSiO_2$ export
- Worldwide, Aulosphaeridae alone may represent a significant proportion of $bSiO_2$ export to the deep mesopelagic ocean (>500 m)

Supporting Information:
- Supporting Information S1
- Figure S1
- Figure S2
- Figure S3
- Table S1
- Table S2

Correspondence to:
T. Biard,
tbiard@ucsd.edu

Citation:
Biard, T., Krause, J. W., Stukel, M. R., & Ohman, M. D. (2018). The significance of giant Phaeodarians (Rhizaria) to biogenic silica export in the California Current Ecosystem. *Global Biogeochemical Cycles*, *32*. https://doi.org/10.1029/2018GB005877

Received 4 JAN 2018
Accepted 13 MAY 2018
Accepted article online 19 MAY 2018

Abstract In marine ecosystems, many planktonic organisms precipitate biogenic silica ($bSiO_2$) to build silicified skeletons. Among them, giant siliceous rhizarians (>500 μm), including Radiolaria and Phaeodaria, are important contributors to oceanic carbon pools but little is known about their contribution to the marine silica cycle. We report the first analyses of giant phaeodarians to $bSiO_2$ export in the California Current Ecosystem. We measured the silica content of single rhizarian cells ranging in size from 470 to 3,920 μm and developed allometric equations to predict silica content (0.37–43.42 μg Si/cell) from morphometric measurements. Using sediment traps to measure phaeodarian fluxes from the euphotic zone on four cruises, we calculated $bSiO_2$ export produced by two families, the Aulosphaeridae and Castanellidae. Biogenic silica export ranged from <0.01 to 0.63 mmol $Si \cdot m^{-2} \cdot day^{-1}$. These two families alone contributed on average 10% (range 0–80%) of total $bSiO_2$ export from the euphotic zone. Their proportional contributions increased substantially in more oligotrophic regions with lower $bSiO_2$ fluxes. Using the in situ Underwater Vision Profiler 5, we characterized vertical distributions of the giant phaeodarian family Aulosphaeridae to a depth of 500 m and inferred their contribution to $bSiO_2$ export in deeper waters. We found a significant increase of Aulosphaeridae export (<0.01 to 2.82 mmol $Si \cdot m^{-2} \cdot day^{-1}$) when extended to mesopelagic depths. Using a global data set of in situ profiles, we estimated the significance of Aulosphaeridae to $bSiO_2$ export and revealed that they can act as major exporters of $bSiO_2$ to the mesopelagic zone in various regions.

1. Introduction

Elucidating the processes responsible for the cycling of macronutrients in the modern ocean is crucial to predicting marine planktonic primary production and the magnitude of carbon dioxide removed from the atmosphere (Ducklow et al., 2001; Eppley & Peterson, 1979; Falkowski et al., 1998). Among other chemical elements in the ocean, silicon has long been of interest to marine scientists and micropaleontologists (Nelson et al., 1995; Ragueneau et al., 2000; Tréguer et al., 1995). Silicic acid is a key macronutrient, essential for the growth of many organisms including diatoms, a group of unicellular phytoplankton with cell walls made of biogenic silica ($bSiO_2$, also known as biogenic opal) that is responsible for up to one fifth of Earth's primary production (Nelson et al., 1995). In addition to diatoms, the production and export of $bSiO_2$ in the ocean can also be attributed, to a lesser extent, to other silicifying organisms, including the pico-cyanobacteria *Synechococcus*, hexactinellid sponges, silicoflagellates, and those rhizarians bearing siliceous skeletons (Tréguer & De La Rocha, 2013). Although a few studies have estimated the quantitative importance of water-column *Synechococcus* to $bSiO_2$ standing stocks and fluxes (Baines et al., 2012; Krause et al., 2017), little is known about the significance of siliceous rhizarians in the marine silica cycle despite their extensive use in micropaleontology (De Wever et al., 2002; Suzuki & Aita, 2011).

Rhizaria, one of the main eukaryotic super-kingdoms, comprise a diverse group of marine amoeboid protists that includes some organisms that build complex skeletons of opaline silica (SiO_2-nH_2O), strontium sulfate, or calcium carbonate (Burki & Keeling, 2014). Only the emblematic polycystine radiolarians and lesser known Phaeodaria incorporate silica into their skeleton (Suzuki & Not, 2015). Formerly referred to as radiolarians, phaeodarians have been recently classified within the phylum Cercozoa (Nakamura et al., 2015; Nikolaev et al., 2004; Polet et al., 2004). Upon death, their siliceous skeletons will likely sink toward the bottom of the ocean and, if not remineralized, eventually be incorporated in seafloor sediments. This process is especially important in the equatorial Pacific where rhizarian silica is a primary component of the siliceous ooze

(Lisitzin, 1972). While polycystine radiolarians have been extensively studied for their fossil records and used as proxies for paleoclimate reconstruction (De Wever et al., 2002; Suzuki & Aita, 2011), phaeodarians are rarely preserved in sediments and have very limited fossil records (reviewed by Nakamura & Suzuki, 2015). Only very favorable conditions promote the preservation of phaeodarian skeletons as fossils (Dumitrica & Van Eetvelde, 2009; Nakamura & Suzuki, 2015; Stadum & Ling, 1969). Consequently, unlike most polycystine radiolarians, it is generally accepted that fossil records do not accurately reflect the significance of phaeodarians and other fragile siliceous rhizarians in overlying waters or their role in the marine silica cycle.

Many planktonic organisms developed mineral structures (e.g., diatoms and tintinnids) that are believed to confer protection against predators (reviewed in Hamm & Smetacek, 2007). Although skeleton-bearing plankton are commonly considered robust organisms, some, such as phaeodarians, possess more delicate skeletons. Unlike polycystine radiolarians, phaeodarians are characterized by a porous siliceous skeleton bearing hollow spicules (Nakamura & Suzuki, 2015). The delicate nature of phaeodarian skeletons is known to affect measures of their abundance and contribution to vertical fluxes. Most phaeodarians are broken upon collection with standard plankton net tows (Nakamura & Suzuki, 2015). Only recent advances in in situ imagery have revealed clear evidence of the substantial contribution of Phaeodaria to oceanic carbon pools (Biard et al., 2016). In addition, in an ocean undersaturated with respect to silica (Stumm & Morgan, 2012), many fragile phaeodarians appear to dissolve when settling through the water column (Erez et al., 1982; Takahashi & Honjo, 1981). Despite these constraints, a handful of studies have investigated phaeodarian vertical fluxes (Abelmann, 1992; Boltovskoy et al., 1993a; Gowing, 1986; Ikenoue et al., 2012; Takahashi, 1987) and, to a lesser extent, their contribution to the marine silica cycle (Bernstein et al., 1990; Takahashi et al., 1983; Takahashi & Honjo, 1981).

Early studies suggested that radiolarians (at the time inclusive of phaeodarians) were the second most important producers of suspended silica in the oceans, even surpassing diatoms in equatorial regions (Lisitzin, 1972). Detailed analyses in the western tropical Atlantic later revealed that radiolarian $bSiO_2$ fluxes (1.2 to 2.5 mg $Si \cdot m^{-2} \cdot day^{-1}$) contribute from 14 to 31% of total $bSiO_2$ export (Takahashi & Honjo, 1981). However, with no assessment of the contribution from phaeodarians independent of polycystine radiolarians, the significance of phaeodarians in the marine silica cycle is still unclear. The only dedicated quantification of phaeodarian $bSiO_2$ fluxes suggested a rather similar range of contribution, with low to moderate percentages (3–23%) of total $bSiO_2$ export (Takahashi et al., 1983). However, these results were based on deep sediment traps moored for a period of months. These estimates are likely to be minimal values, due to the delicate nature of their skeletons and likelihood of dissolution, even at low temperatures. In addition to the paucity of phaeodarian flux data, previous studies focused mostly on small phaeodarians ($<$500 μm), leaving unknown the contribution of larger taxa, which may have significantly more silica per cell. While most phaeodarian species are a few hundred micrometers across (Nakamura & Suzuki, 2015), some, the giants, can exceed a few millimeters in size (e.g., Aulosphaeridae or Tuscaroridae; Ling & Haddock, 1997). Initial assessment of the silica content of these giants revealed extremely high values (12–73 μg Si/cell), 1 or 2 orders of magnitude higher than the average silica content for small siliceous rhizarians (Takahashi, 1981) and about 4 orders of magnitude higher than marine diatoms (average ≈ 0.0089 μg Si/cell; Conley et al., 1989). Because of their high silica content, larger size, and significantly faster sinking speed than smaller species ($>$500 m/day for cells larger than 240 μm, compared to 50–200 m/day for smaller cells; Berger, 1976), these giants are likely to influence the marine silica cycle by rapidly transporting appreciable amounts of $bSiO_2$ to the deep ocean (Takahashi et al., 1983). Similarly, giant diatoms have proven to be efficient vectors of elemental fluxes to the deep ocean, contrasting with smaller species (Smetacek, 2000). However, the impact of these giant phaeodarians on the marine silica cycle has never been directly investigated. Given their new-found importance to plankton biomass (Biard et al., 2016), these giants potentially represent a significant link between the biogeochemical cycles of carbon and silicon. But more importantly, if these organisms do represent a significant proportion of deep $bSiO_2$ export, such an interpretation would call for re-evaluating the utility of using $bSiO_2$ export to infer diatom contribution to carbon export (Honjo et al., 2008).

Here we investigate the contribution and significance of giant phaeodarians to the marine silica cycle along a gradient of hydrographic conditions across the California Current Ecosystem (CCE). We first collected single-cell specimens of siliceous rhizarians in order to quantify their silica content. Then we used sediment trap material, collected between 2011 and 2016 from four research cruises of the CCE Long-Term Ecological

Research (LTER) program (Ohman et al., 2013), to measure vertical fluxes and $bSiO_2$ export mediated by giant phaeodarians and to assess their contribution to total $bSiO_2$ export out of the euphotic zone. Additionally, we used in situ imagery (Underwater Vision Profiler 5 [UVP5]; Picheral et al., 2010) to quantify their vertical distributions to 500 m depth and to infer deeper fluxes of one giant phaeodarian family, the Aulosphaeridae. We also provide the first global estimates of the contribution of the Aulosphaeridae to deep $bSiO_2$ export into mesopelagic depths.

2. Material and Methods

2.1. Single-Specimen Quantification of Silica Content

Siliceous rhizarian specimens (Phaeodaria and polycystine Radiolaria) were handpicked from fresh plankton samples or sediment trap material (supporting information Figure S1). Plankton samples were collected gently between April and June 2017, off the Scripps Pier in the La Jolla Canyon (USA, 32°52′01″N, 117°15′26″W) and off Catalina Island (33°06′43″N 118°06′27″W), using either a 202 μm mesh bongo net or a 333 μm ring net in oblique tows (0–200 m). Phaeodarian specimens from sediment traps were collected in 2016 (Process Cruise CCE-P1604) off Point Conception, California. Handpicked living specimens were rinsed and manually cleaned in 0.8 μm filtered seawater and subsequently imaged with light microscopy. To prevent carryover of silicic acid in the rinse, clean specimens were then rinsed with a NaCl solution (3.3% w/v) and finally oven dried at 65°C for 30 min or until water evaporated completely.

Single-cell silica analysis of rhizarians was done by modifying frequently used methods. Specimens were immersed in 0.2 ml of a 2.5 N hydrofluoric acid solution, immediately capped, and placed in a fume hood. Rhizarian silica was allowed to digest at room temperature (20–22°C) for 48 hr as is typically done for lithogenic silica analysis. After digestion, half the volume was diluted with saturated boric acid to complex the hydrofluoric acid, and the solubilized rhizarian silica was analyzed spectrophotometrically using a manual and sensitive colorimetric analysis (e.g., Krause et al., 2017) using standards made in a similar boric acid and hydrofluoric acid matrix. While previous silica content measurements on siliceous rhizarians (e.g., Takahashi, 1981) have used a sodium carbonate fusion of silica in a crucible to produce sodium metasilicate (which easily dissolves in seawater), that method has a lower throughput and requires more handling. Our method was modified from a similar approach for measuring silica content of the giant diatom *Ethmodiscus* spp. (cell volume $> 10^9$ μm^3) in the North Pacific gyre (Villareal et al., 1999). Using our method, the average rhizarian silica in the analyzed solution was ~100-fold higher than detection limits.

Morphometric measurements were performed for each specimen using ImageJ (supporting information Table S1). The length of *A. scolymantha* and specimens of the Castanellidae was calculated as the maximum length of the scleracoma (i.e., not taking into account longer radial spines), while for Coelodendridae specimen length was measured as the length of the longest dimension including radial spines. For the special case of *N. valvidiae*, length was taken as the longest distance between two opposite floats, and not two opposite radial spines. Measurements of width followed the same rationale. For Aulosphaeridae, we additionally measured the % silicified area, estimated as the ratio between silicified structures and the total surface area (including empty or nonsilicified parts). In triplicate, we measured areas of both silicified and nonsilicified regions within squares of 200 to 500 μm^2 and estimated the % silicified area. Finally, for Aulosphaeridae specimens, we measured the thickness of silicified tubes. For all specimens, including those derived from the literature, we estimated biovolume using the most appropriate geometrical model (e.g., sphere, ellipsoid, cone, and disk). Additionally, for the Aulosphaeridae, we estimated the biovolume represented by the silicified parts, using % silicified area and tube thickness, applied to an empty ellipse model.

2.2. Process Cruise Design

Samples for this study were collected on four process cruises of the CCE-LTER program (supporting information Figure S2). During P1106 (June 2011) and P1208 `August 2012) cruises addressed the biogeochemical impact of mesoscale features (fronts and eddies). Consequently, measurements were focused in areas within and on either side of distinct oceanographic features (Krause et al., 2015; Ohman et al., 2013; Stukel et al., 2017). During P1408 (August 2014) sampling was conducted in the same region, across anomalously warm, stratified waters probably associated with an intrusion of subtropical water. For P1604 (April 2016) the primary cruise goal was to investigate the regional impact of the El Niño of 2015–2016 (Jacox et al., 2016). A

range of study sites was sampled, from the coastal upwelling region near Point Conception to offshore locations with communities that more closely resemble those of the oligotrophic gyre.

On all cruises, measurements were carried out during quasi-Lagrangian experiments of two- to five-day duration (Landry et al., 2009). During these experiments, water parcels of interest were identified using a free-fall Moving Vessel Profiler (Ohman et al., 2012) and subsequently marked and followed using two drifting arrays (Landry et al., 2009). We designate each followed water parcel a "Cycle," signifying repeated cycles of experimental measurements in the same water parcel. One of the arrays had sediment traps deployed at the base of the euphotic zone (if shallower than 80 m), at 100 m, and 150 m (on P1604 and P1408 only). During these Lagrangian experiments, we also conducted at least twice daily vertical profiles with a CTD-rosette with an attached UVP5.

2.3. Sediment Trap Deployment

Vertical fluxes of particulate silica and giant phaeodarians were measured using VERTEX-style particle interceptor trap (PIT) cylindrical sediment traps with a 70 mm internal diameter, 8:1 aspect ratio, and a baffle constructed of 13 smaller, beveled tubes with similar 8:1 aspect ratio (Knauer et al., 1979). Between 8 and 12 PIT tubes were deployed on cross-pieces at one to three depths on a drifting sediment trap array. The array also included a surface float with Globalstar communications and a 3×1 m holey sock drogue that was centered at a depth of 15 m (Stukel et al., 2013). PIT tubes were filled with a preserved brine consisting of 0.1 μm filtered seawater, 50 g/L NaCl, and 0.4% formaldehyde. Deployment duration varied from two to five days (supporting information Table S2). Simultaneous ^{238}U-^{234}Th deficiency measurements made on these cruises and on previous cruises in the CCE-LTER program have shown excellent agreement between ^{234}Th fluxes and fluxes from these VERTEX-style sediment traps, suggesting that any hydrodynamic biases are minimal (Stukel et al., 2013, 2015).

After recovery, overlying seawater above the trap brine was immediately removed by gentle suction and samples gravity filtered through a 200 μm mesh filter (47 mm diameter). Under a stereomicroscope, swimming mesozooplankton that were believed to have been transported into the trap during active vertical migrations (i.e., not by sinking) were removed from the filter. Abundances of giant Phaeodaria (Castanellidae and Aulosphaeridae) were also enumerated on each filter. Smaller radiolarian and phaeodarian taxa were occasionally observed but not enumerated, as a substantial fraction was not retained by the 200 μm mesh. Microscopic analyses of all samples were typically completed within 24 hr of sediment trap recovery to minimize potential dissolution of Phaeodaria.

2.4. Biogenic Silica Export Estimation

Biogenic silica export was measured using previously described methods used in the CCE-LTER (Krause et al., 2015). After quantification of phaeodarian abundance and swimmer removal, the contents of the filters were rinsed back into the original sample (i.e., $>$200 and $<$200 μm material was recombined). A rotary Folsom splitter was used to subsample from different tubes at each deployment depth. The fractional split from the sediment trap was filtered onto a 0.6 μm, 47 mm polycarbonate membrane filter and dried at 60°C for 24 hr (or until dry). In the lab, $bSiO_2$ was analyzed using NaOH digestion as described previously for CCE-LTER samples (Krause et al., 2015). During the P1106 cruise, sediment trap brine was collected before and after deployment to determine dissolution of $bSiO_2$ during the collection period. Dissolution of $bSiO_2$ during collection was highest when the absolute $bSiO_2$ flux was lowest (i.e., up to 10% of the particulate flux); however, in deployments showing higher $bSiO_2$ flux, $bSiO_2$ dissolution was typically $<$2%. For all cruises after P1106, $bSiO_2$ dissolution was not assessed, as the fraction of dissolution relative to the particle flux was much lower than the variability among collection tubes at a given depth.

2.5. In Situ Assessment of Giant Phaeodarian Standing Stock

The community of giant phaeodarians was quantified in situ using the UVP5, an in situ imaging system capable of recording images of large planktonic organisms (equivalent spherical diameter, ESD $>$600 μm; Picheral et al., 2010). The UVP5 was mounted on the bottom of the CTD-rosette frame to limit flow perturbation and we sampled only from the downcast. With a sampling volume of 0.5–1 L, the UVP5 takes one image every 5 to 20 cm (depending on the imaging frequency, 10–15 Hz) and provides a mean observed volume of 5 m^3 for a 0–500 m vertical profile. Between 2011 and 2016, the UVP5 was deployed for 1,045 vertical profiles

Table 1
Silica Content and Morphometric Measurements of Siliceous Rhizarians

Species[a]	n	Length (μm)		Silica[b] (μg Si/cell)		Reference
		Min-max	Mean	Min-max	Mean[c]	
Nassellaria						
Androspyris reticulidisca	–	284–420	363 ± 45	–	0.671	Takahashi (1981)
Anthocyrtidium ophirense	–	183–214	191 ± 12	–	0.147	Takahashi (1981)
Conicavus tipiopsis	–	343–816	567 ± 89	–	0.524	Takahashi (1981)
Eucyrtidium acuminatum group	–	164–325	248 ± 43	–	0.336	Takahashi (1981)
Lamprocyclas maritalis maritalis	–	201–280	229 ± 22	–	0.497	Takahashi (1981)
Litharachnium tentorium	2	890–1000	945 ± 78	0.37–0.58	0.47 ± 0.15	This study
Nephrospyris renilla	–	338–529	413 ± 71	–	1.048	Takahashi (1981)
Spirocyrtis scalaris	–	158–263	209 ± 23	–	0.044	Takahashi (1981)
Spumellaria						
Actinomma arcadophorum	–	230–300	269 ± 26	–	0.703 ± 0.081[c]	Takahashi (1981)
Dictyocoryne profunda > 350 μm	–	374–508	424 ± 33	–	1.561 ± 0.029[c]	Takahashi (1981)
Dictyocoryne profunda < 350 μm	–	206–376	294 ± 42	–	0.766 ± 0.057[c]	Takahashi (1981)
Dictyocoryne elegans[a]	–	303–450	369 ± 43	–	0.451 ± 0.157[c]	Takahashi (1981)
Dictyocoryne profunda[a]	–	250–395	308 ± 43	–	1.846 ± 0.018[c]	Takahashi (1981)
Myelastrum trinibrachium	–	912–1224	1027 ± 120	–	0.658	Takahashi (1981)
Spongodiscus sp. >270 μm[a]	–	257–401	313 ± 38	–	0.766 ± 0.187[c]	Takahashi (1981)
Spongotrochus glacialis	–	173–304	236 ± 36	–	0.343 ± 0.040[c]	Takahashi (1981)
Collodaria						
Polysolenia murrayana[a]	–	116–219	176 ± 18	–	0.47 ± 0.031[c]	Takahashi (1981)
Collosphaera huxleyi	–	–	–	–	0.3	Bernstein et al. (1990)
Phaeodaria						
Aulacantha scolymantha	19	550–980	698 ± 105	0.40–4.39	1.80 ± 1.29	This study
Aulosphaeridae spp.					10.90 ± 5.9	This study
Auloscena spp.	15	1480–2780	2335 ± 293	4.53–19.21	12.39 ± 5.19	This study
Aulosphaera spp.	13	1132–2920	1816 ± 574	3.69–23.74	9.18 ± 6.4	This study
Castanidium abundiplanutum	–	271–330	308 ± 21	–	0.54	Takahashi (1981)
Castanidium longispinum	–	–	470 ± 34	–	2.132 ± 0.346[c]	Takahashi (1981)
Castanellidae sp.	9	470–700	614 ± 92	11.63–16.64	14.54 ± 1.99	This study
Challengeria tizardi	-	317–373	340 ± 25	–	0.482	Takahashi (1981)
Coelodendridae sp. 1	1	-	3300	–	17.80	This study
Coelodendridae sp. 2	5	683–830	730 ± 59	2.11–3.66	2.64 ± 0.63	This study
Conchellium tridacna	–	–	–	–	7.9	Bernstein et al. (1990)
Conchidium argiope	–	160–216	196 ± 14	–	0.058	Takahashi (1981)
Conchopsis compressa	–	539–622	587 ± 28	–	2.353 ± 0.244[c]	Takahashi (1981)
Entocannula subglobosa	–	–	–	–	6.5	Bernstein et al. (1990)
Haeckeliana porcellana	–	324–563	407 ± 54	–	5.842 ± 2.104[c]	Takahashi (1981)
Nationaletta valvidiae	1	–	3920	–	43.42	This study
Protocystis curva	–	174–185	180 ± 6	–	0.107	Takahashi (1981)
Protocystis naseri var. *ovalis*	–	–	–	–	10.7	Bernstein et al. (1990)
Protocystis thomsoni	–	–	–	–	3.7	Bernstein et al. (1990)
Tuscaretta belknapi	–	–	–	–	64	Bernstein et al. (1990)
Tuscaretta globosa	–	–	–	–	59.6	Bernstein et al. (1990)
Tuscarettta tubulosa	–	–	–	–	57.9	Bernstein et al. (1990)

Note. Mean values are given as mean ± standard deviation (SD).
[a]Species and genus identifications from Takahashi (1981) have been updated according to Matsuzaki et al. (2015). [b]Conversion from nmol Si/cell to μg Si/cell assuming a molecular of weight of 67 g/mol for hydrated amorphous silica (Mortlock & Froelich, 1989). [c]Mean ± 2 SD for values from Takahashi (1981).

sampling from 0 to 500 m and generated 745,963 vignettes (i.e., individual images of regions of interest larger than 600 μm). These data were analyzed as described in Biard et al. (2016). Briefly, vignettes were extracted using ZooProcess software (Gorsky et al., 2010), automatic morphometric measurements were performed on each vignette, and a computer-assisted method ultimately assigned vignettes to a taxonomic framework. All classifications were then manually validated. Rhizaria accounted for 15,568 vignettes, identified to different taxonomic level, including different families of Phaeodaria, but also Acantharia, Collodaria, and Foraminifera. All sorted vignettes have been deposited online at Ecotaxa (http://ecotaxa.obs-vlfr.fr) and are available upon request (Picheral, 2017).

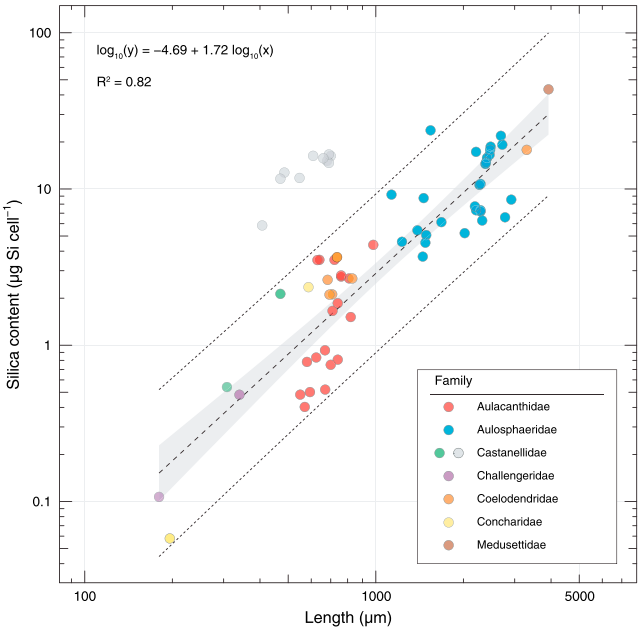

Figure 1. Relationship between silica content (Si; µg Si/cell) and cell length (L; µm) across marine phaeodarians. For phaeodarians, excluding the shaded grey points (Castanellidae and *H. porcellana*), the silica content varies as $\log_{10}$ (Si) = −4.69 + 1.72 $\log_{10}$(L) as estimated by a linear regression (dashed line) with 95% confidence interval (gray band) and prediction interval (dotted line). Detailed values in Table 1.

2.6. Data Analysis

Data analyses were conducted using R 3.4.1. (R Core Team, 2017), the *tidyverse* package (Wickham & RStudio, 2017) and custom scripts. Allometric equations between morphometric measurements and silica content were tested using both Models I and II linear regressions using the *lmodel2* package (Legendre, 2014). However, we report the Model I regressions because values of the independent variable were measured with minimal error and our objective was to develop predictive regression relationships. If not otherwise specified, data were log-transformed ($\log_{10}$ or $\log_{10}$ [$x+1$]) prior to linear regression, with assumptions confirmed using the *gvlma* package in R (Pena & Slate, 2014).

UVP5 vignette morphometric measurements, extracted during the ZooProcess image processing, were used to estimate biovolume of the different phaeodarian categories. For all phaeodarian vignettes, except the ones displaying long pseudopodial-like extensions, biovolume was calculated using the major and minor axis of the best fitting ellipse. For the biovolume of phaeodarians with pseudopodial-like extensions, we used the ESD to calculate the volume of a sphere, thereby avoiding overestimation due to long extensions.

3. Results

3.1. Quantification of Silica Content in Marine Siliceous Rhizarians

We quantified silica content for 65 specimens of siliceous rhizarians collected from net tows and sediment traps (Table 1, supporting information Table S1 and Figure S1). Analyzed specimens belonged primarily to the order Phaeodaria, in addition to two specimens of the order Nassellaria. To make direct comparisons with literature values, we expressed silica content as µg Si/cell assuming a molecular weight of 67 g/mol for hydrated amorphous silica (Mortlock & Froelich, 1989). Overall, silica content varied over 2 orders of magnitude (0.37–43.42 µg Si/cell), lowest for the nassellarian *Litharachnium tentorium*, and highest for the colonial phaeodarian *Nationaletta valvidiae* (specimen composed of four individual cells connected together). On average, the highest silica content was obtained for the family Castanellidae (14.54 ± 1.99 µg Si/cell; mean ± standard error [SE]), with low interspecimen variability. The family Aulacanthidae, represented by *Aulacantha scolymantha*, displayed the lowest average silica content of phaeodarians collected in this study (1.8 ± 1.29). The family Aulosphaeridae displayed highly variable silica content (10.9 ± 5.9) with a small difference between the two genera *Auloscena* and *Aulosphaera*, 12.39 ± 5.19 and 9.18 ± 6.4, respectively, the latter having smaller cell length and a reduced silicified area (supporting information Table S1). The third family, Coelodendridae, showed markedly different mean silica content between the two morphotypes: 17.8 for the first morphotype (sp1) and 2.64 ± 0.63 for the second (sp2). This difference in silica content was consistent with differences in cell length between morphotypes (3,300 and 730 ± 59 µm, respectively).

We compare our estimates of phaeodarian silica content with published values in Table 1 and Figure 1. Literature values mostly include smaller specimens (116–1,027 µm, mean = 353 µm) than the present data (470–3,920 µm, mean = 1,388 µm), making it difficult to compare values between sources. Direct comparison of similar taxa was only possible for present specimens belonging to the family Castanellidae and previous analyses of *Castanidium longispinum* and *Haeckeliana porcellana* (Takahashi, 1981). Although we could not identify our species with certitude, *H. porcellana* has a dense skeleton morphology similar to our specimens and showed similar silica content. However, *C. longispinum*, which also had a similar morphology, had appreciably lower silica content than the previously analyzed Castanellidae specimens.

We evaluated allometric equations to test the hypothesis that the phaeodarian silica content is related to cell size. Over a size range from 176 to 3,920 µm, phaeodarian silica content could be predicted from cell length (Figure 1; $R^2 = 0.82$, $F(1,58) = 272$, $P < 0.001$) from

$$\log_{10}(\text{silica content}) = -4.69 + 1.72\ \log_{10}(\text{length}) \quad (1)$$

where silica content is in units of μg Si/cell and length in μm. This relation excludes the Castanellidae from the present study, which had unusually high silica content, as well as the literature value for *H. porcellana* that displayed a denser skeleton and appeared outside of the 95% prediction interval (gray symbols in Figure 1). A significant log-log linear relationship ($R^2 = 0.82$, $F(1,58) = 271$, $P < 0.001$) was also obtained when expressed as a function of cell biovolume spanning four orders of magnitude (0.0019–26.45 mm^3):

$$\log_{10}(\text{silica content}) = -4.32 + 0.56\ \log_{10}(\text{biovolume}) \quad (2)$$

where silica content is in units of μg Si/cell and biovolume in μm^3.

We tested an additional linear regression by weighting the biovolume of each Aulosphaeridae specimen by its estimated silica coverage (% area as silica) and found a significant relationship, although with relatively low predictive power ($R^2 = 0.23$, $F(1,26) = 7.702$, $P < 0.05$). Finally, when considering the 88 known values of silica content for marine siliceous rhizarians, including 23 nassellarians, spumellarians, collodarians, and phaeodarians from a previous study (Table 1), silica content could also be predicted from cell length ($R^2 = 0.57$, $F(1,86) = 116$, $P < 0.001$; supporting information Figure S3):

$$\log_{10}(\text{silica content}) = -3.77 + 1.44\ \log_{10}(\text{length}) \quad (3)$$

or from cell biovolume ($R^2 = 0.64$, $F(1,85) = 149$, $P < 0.001$):

$$\log_{10}(\text{silica content}) = -3.51 + 0.47\ \log_{10}(\text{biovolume}) \quad (4)$$

3.2. Vertical Fluxes of Giant Phaeodarians and Their Contributions to Biogenic Silica Export

Across water parcels sampled on the four cruises, export of $bSiO_2$ from the euphotic zone of the CCE ranged from 0.14 to 19.34 mmol $Si \cdot m^{-2} \cdot day^{-1}$ (Figure 2a, supporting information Table S2). The highest cycle-specific export (19.34 ± 0.86; mean ± SE) and cruise-average export of $bSiO_2$ (5.64 ± 0.29; mean ± SE) were both recorded in 2011, while we measured lower $bSiO_2$ export in subsequent cruises. Intracruise variability in $bSiO_2$ flux was greater than the variability among cruises. We observed a clear pattern of increasing $bSiO_2$ export toward regions of higher primary productivity (gradient left to right, Figures 2a and 2c). This pattern was consistent across the four cruises sampled. Averaged across the cycles, we found no significant attenuation of $bSiO_2$ flux with depth in the epipelagic. Indeed, $bSiO_2$ flux at 100 or 150 m depth was often greater than $bSiO_2$ flux at the base of the euphotic zone (Figure 2a).

We then quantified vertical fluxes of two families of giant phaeodarian, Aulosphaeridae and Castanellidae (representative micrographs displayed in Figure 3). Their fluxes captured by sediment traps ranged from 0 to 2,439 $ind \cdot m^{-2} \cdot day^{-1}$ and 0 to 1,458 $ind \cdot m^{-2} \cdot day^{-1}$, respectively (supporting information Table S2). To assess their individual and combined contributions to the total $bSiO_2$ export from the euphotic zone, we converted the number of sinking specimens ($ind \cdot m^{-2} \cdot day^{-1}$) to quantities of sinking $bSiO_2$ (mmol $Si \cdot m^{-2} \cdot day^{-1}$). We used the newly measured average silica contents (Table 1): 14.54 μg Si/cell or 0.22 μmol Si/cell for the Castanellidae and 10.9 μg Si/cell or 0.16 μmol Si/cell for the Aulosphaeridae. Overall, the $bSiO_2$ exported from the euphotic zone of the CCE by the two phaeodarian families was higher for the Aulosphaeridae (0.074 ± 0.013 mmol $Si \cdot m^{-2} \cdot day^{-1}$; mean ± SE) compared to the Castanellidae (0.043 ± 0.012; supporting information Table S2). Intercruise $bSiO_2$ export mediated by the two families showed no consistent spatial pattern over the areas sampled (supporting information Figure S4). Biogenic silica export of Aulosphaeridae appeared more variable over time and space than the export driven by the Castanellidae. When considering $bSiO_2$ export to different depths, we usually observed an increase of export with depth for both families.

When compared to the total $bSiO_2$ export, the combined contribution of Aulosphaeridae and Castanellidae averaged 10% over the four years sampled, with the Aulosphaeridae responsible for more than half of the combined contribution (Figure 2b). Their maximum contribution was measured locally at 100 m on Cycle 5 in 2011, reaching up to 80% of the total $bSiO_2$ export in this region of low $bSiO_2$ export (0.25 mmol $Si \cdot m^{-2} \cdot day^{-1}$). Averaged across all Cycles on a cruise, the two phaeodarian families together reached their highest contribution in 2011 and 2016, constituting 17% and 18% of the total $bSiO_2$ export, respectively. While we measured half this level of contribution in 2012, both the Aulosphaeridae and

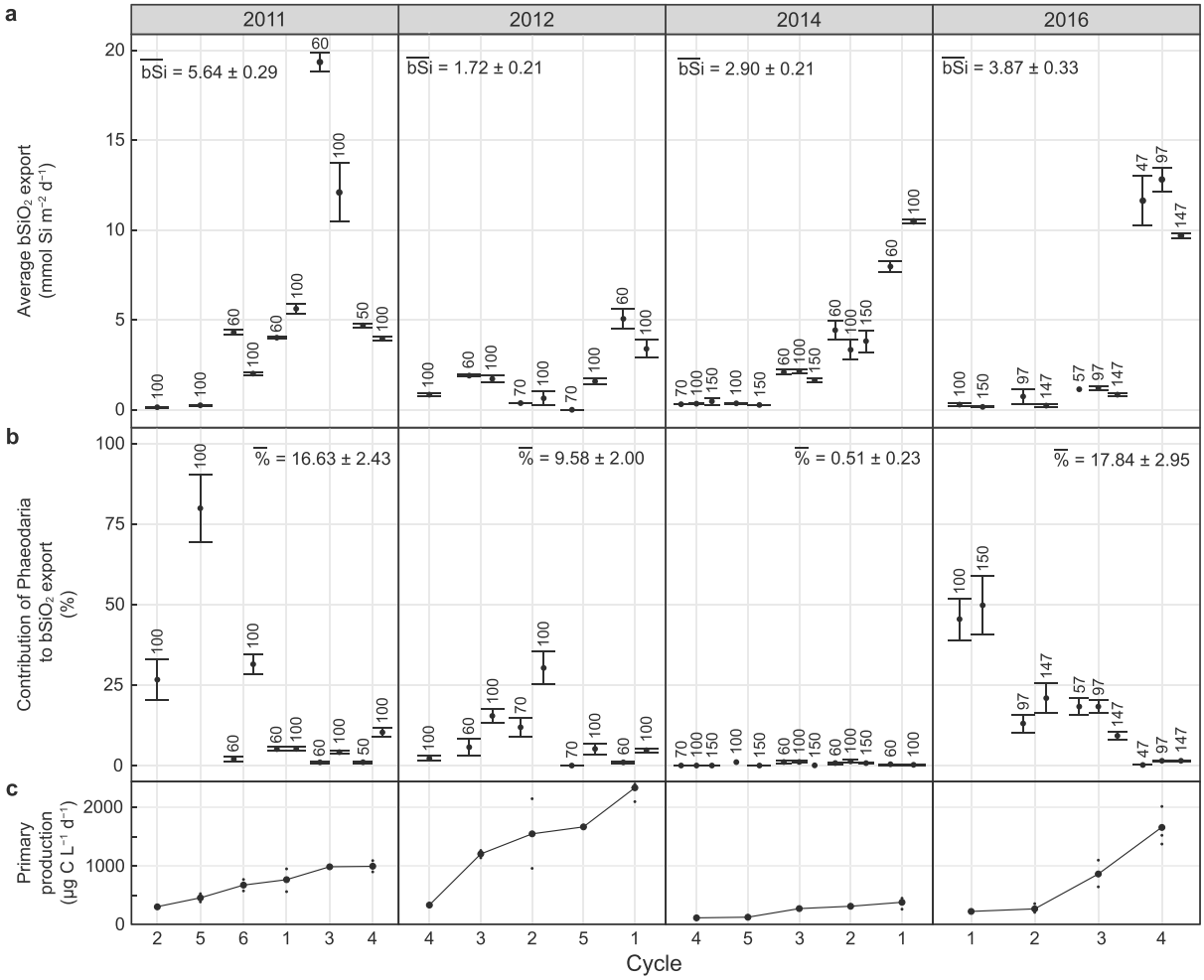

Figure 2. Contribution of giant phaeodarians (Aulosphaeridae and Castanellidae) to total $bSiO_2$ export (mmol Si · m^{-2} · day^{-1}) across four cruises (2011, 2012, 2014, and 2016) in the California current ecosystem. (a) Variation of total $bSiO_2$ export. Values are means of duplicate/triplicate measurements. (b) Combined contribution (%) of Aulosphaeridae and Castanellidae to total $bSiO_2$ export. Mean values ± SE for each cruise are displayed on the top left. Depth of sediment trap deployment (in m) is indicated above each point. (c) Lagrangian Cycles are ordered from left to right along a gradient of increasing primary productivity for each cruise (measured from ^{14}C uptake; Goericke, 2017). Larger dots show means; smaller dots show individual values. Detailed values in supporting information Table S2.

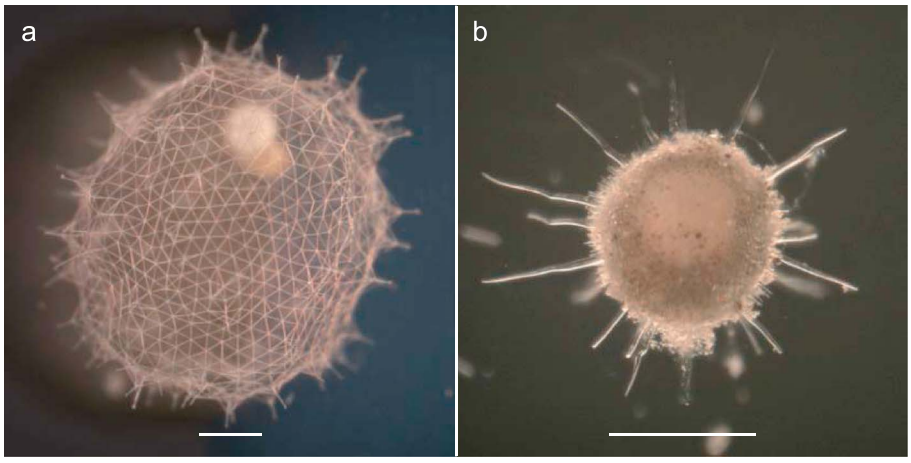

Figure 3. Micrographs of representative giant Phaeodaria from the families (a) Aulosphaeridae and (b) Castanellidae collected from the California Current Ecosystem. Scale bar = 500 µm.

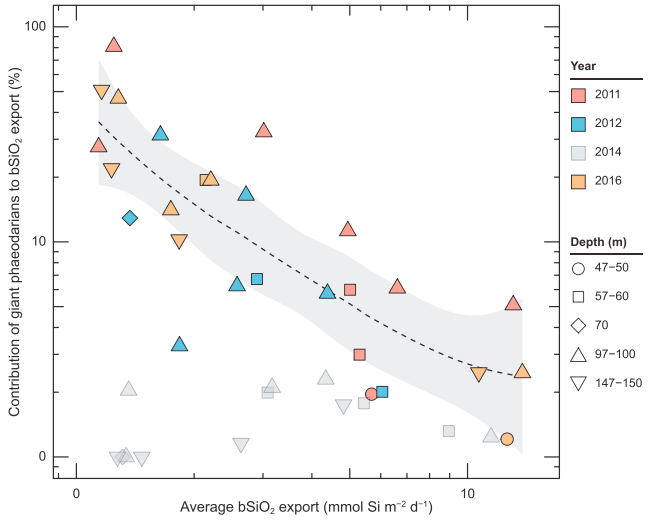

Figure 4. Variation of the contribution of giant phaeodarians to total $bSiO_2$ export with increasing $bSiO_2$ export in the CCE region. The analysis did not include data from 2014 (shaded grey shapes) due to the abnormally depleted rhizarian population. The dashed line indicates loess regression slope; the shading represents the 95% confidence interval.

Castanellidae represented a very small fraction (>0.5%) of the total $bSiO_2$ export in 2014. This insignificant contribution of phaeodarians in 2014 coincided with an overall low C-based primary production of the area sampled (Figure 2c), as well as low phaeodarian vertical fluxes for both families (supporting information Figure S4).

When ordered along a gradient of primary production (Figure 2c), the contribution of these families to the total $bSiO_2$ export showed a pronounced increase with decreasing primary production. There was also a strong increase in the contribution of giant phaeodarians to $bSiO_2$ export toward regions of reduced $bSiO_2$ export (Figure 4). For this analysis, we excluded flux data from 2014 (shaded grey dots) that represent abnormal conditions, as stated previously, deviating from the patterns observed in three other cruises (i.e., more typical conditions).

3.3. In Situ Assessment of Giant Phaeodarian Biogenic Silica Export to the Deep Ocean

In addition to measuring fluxes into sediment traps, the community of suspended giant phaeodarians was measured in situ using the UVP5 (Figure 5). Only the Aulosphaeridae were considered for this analysis, as the Castanellidae were too small to be detected reliably by the camera (threshold = 600 μm). Cruise mean (±SE) integrated abundances of Aulosphaeridae recorded in situ in the first 500 m ranged from 888 ± 124 ind/m^2 in 2014 to 32,750 ± 2,724 ind/m^2 in 2011, with an overall mean abundance of 9,949 ± 1,296 ind/m^2. On average, Aulosphaeridae abundances integrated over the upper 100 and 200 m represented 26% and 81% of the abundance integrated to 500 m, respectively. Consistent with the low vertical fluxes recorded by the sediment traps in 2014 (supporting information Figure S4), in situ quantification of Aulosphaeridae revealed low abundances in the water column, underscoring the need to treat the data from this cruise separately. Detailed vertical distributions of Aulosphaeridae were consistent over the cruises and revealed a sharp increase in abundance between 100 and 200 m (Figure 5). The depth of the maximum Aulosphaeridae abundance (125 ± 8 m) appeared stable throughout the cruises despite the differences in abundance. By comparing the depths of sediment traps with the vertical distribution of Aulosphaeridae, we found that, on average, only 3% of the 0–500 m integrated Aulosphaeridae community was shallower than our 50–60 m traps, 23% was shallower than our 100 m traps, and up to 57% was shallower than our 150 m traps (Figure 5).

With simultaneous deployments of sediment traps and the UVP5, we were able to compare integrated abundances (i.e., standing stocks) of Aulosphaeridae with contemporaneous sediment trap-derived vertical fluxes. We found a strong positive correlation, $R(25) = 0.69$, $P < 0.001$, between standing stocks assessed in situ and vertical fluxes (Figure 6a). As noted, data from 2014 were not considered. However, their inclusion fitted the same pattern, even strengthening the correlation: $R(38) = 0.84$, $P < 0.001$. Considered over all cruises, with the exception of 2014, the inferred median sinking speed of the Aulosphaeridae bulk community, defined as the product of vertical fluxes (ind $\cdot$ m^{-2} $\cdot$ day^{-1}) times the depth of the sediment trap (m), divided by the standing stock above the sediment trap (ind/m^2), was found to be 23 m/day (95% confidence interval = 17–36). When considering the effect of depth on the inferred sinking speed, we found no significant differences between inferred sinking speeds at the three different main depths of trap deployment (Kruskal-Wallis test, $P = 0.8$) with a median speed of 27 m/day at 57–60 m, 22 at 97–100 m, and 32 at 147–150 m (Figure 6b). With an average inferred sinking speed of 16 m/day, inclusion of data from 2014 would not change the present pattern. Additionally, we estimated the median turnover time (d), defined as the ratio between UVP standing stock and sediment trap fluxes, to be 4 days (95% confidence interval = 2–5).

We inferred export of Aulosphaeridae $bSiO_2$ for deeper layers (0–200 m and 0–500 m) using the data acquired in situ by the UVP5 and the newly developed allometric equations. Considering a median inferred sinking speed of 23 m/day, we estimated the Aulosphaeridae $bSiO_2$ export at each cycle matching with sediment trap deployments (Figure 7). When compared to the $bSiO_2$ export estimated from sediment traps,

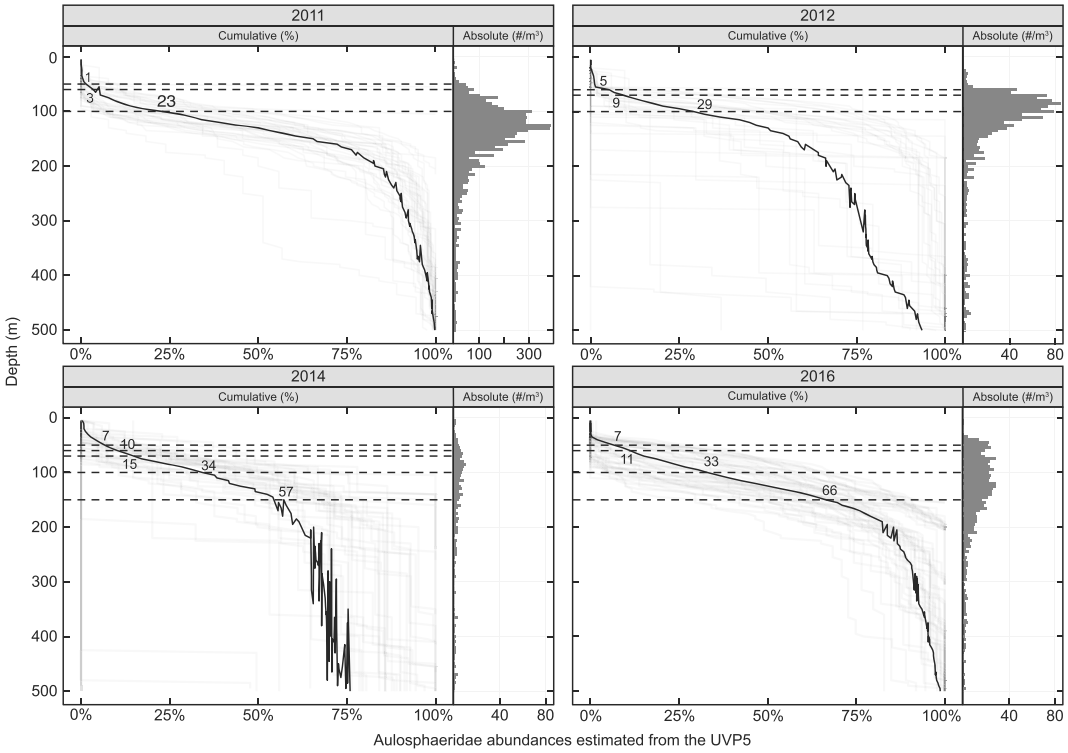

Figure 5. In situ Underwater Vision Profiler 5 vertical profiles of Aulosphaeridae standing stocks in the CCE in 2011, 2012, 2014, and 2016. For each year, the left panel displays the cumulative frequency distribution of Aulosphaeridae abundances as a function of depth. Each light gray line represents a single vertical UVP profile, while the solid black lines display the average trend within each cruise. The dashed lines indicate the deployment depths of sediment traps. Values at the intersection between the dashed lines and the solid lines indicate the average percentage of Aulosphaeridae sampled at that depth. The right panel shows the vertical distribution of concentrations of Aulosphaeridae with 5 m vertical resolution. Note the different scaling for concentrations in 2011.

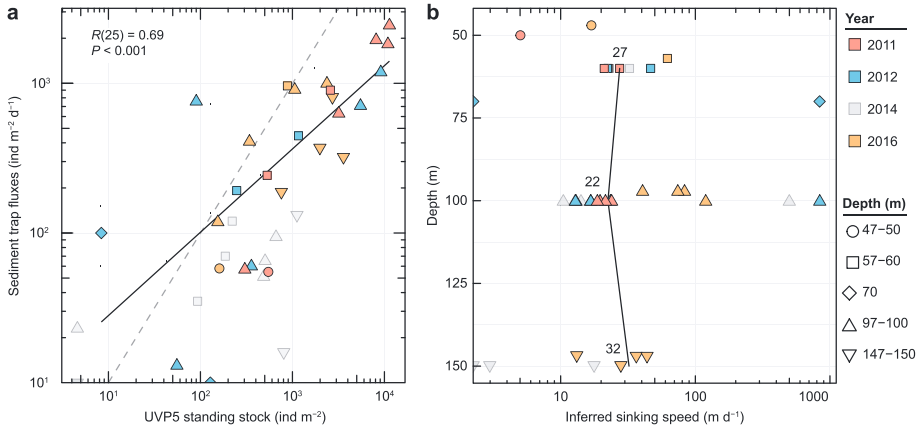

Figure 6. Comparisons between vertical fluxes and in situ standing stocks of Aulosphaeridae. (a) Relationship between vertical fluxes captured by sediment traps and standing stocks of Aulosphaeridae assessed by Underwater Vision Profiler 5. The correlation coefficient (*r*) and its associated probability (*p*) are indicated. The dashed line indicates a 1:1 relationship. (b) Variation of the inferred bulk sinking rate (sediment trap fluxes × depth of integration/UVP5 standing stock) with depth. Median values are shown at 57–60 m, 97–100 m, and 147–150 m. Difference in depths is represented by the different symbol shapes and years by colors. Neither analysis included data from 2014 (shaded grey shapes) due to the abnormally depleted rhizarian population.

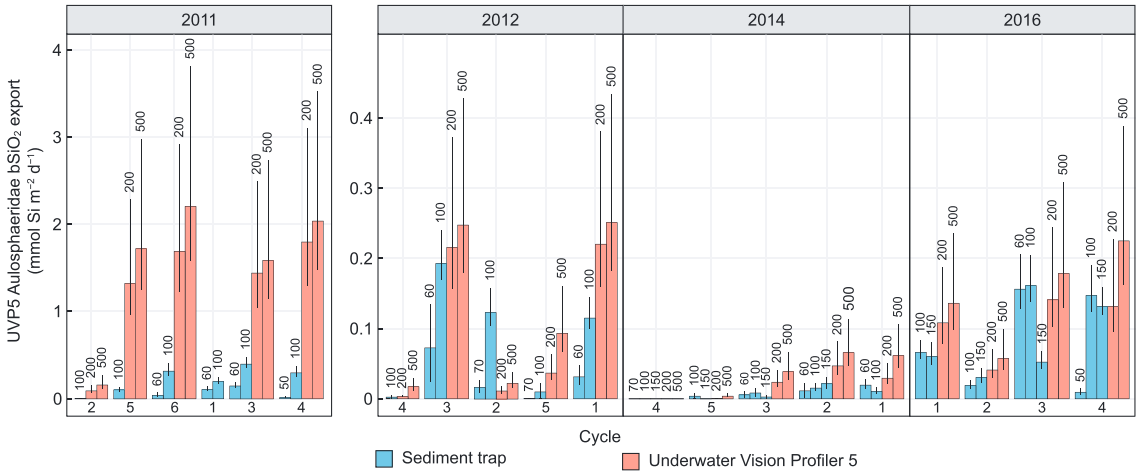

Figure 7. Aulosphaeridae $bSiO_2$ export (mean ± SE) assessed from sediment traps (at 50–150 m depth, blue bars) and in situ measurements using the Underwater Vision Profiler 5 (UVP5, to 200–500 m, salmon bars) in 2011, 2012, 2014, and 2016. Depth of integration is indicated above each bar. Lagrangian Cycles are ordered from left to right along a gradient of increasing primary productivity for each cruise (measured from ^{14}C uptake; Goericke, 2017).

estimated fluxes at 200 and 500 m were nearly always much higher than for shallower depths. Across all cruises, $bSiO_2$ export recorded for the deepest sediment trap (100 or 150 m) accounts for a small-to-moderate portion of the export estimated at 500 m: 13% in 2011, 37% in 2012, 14% in 2014, and 46% in 2016. On average, $bSiO_2$ export estimated by the UVP at 200 and 500 m was higher in 2011, with 1.35 and 1.61 mmol $Si \cdot m^{-2} \cdot day^{-1}$, at the two respective depths. The three following years had significantly lower average $bSiO_2$ export in the deep layers: 0.09 and 0.12 mmol $Si \cdot m^{-2} \cdot day^{-1}$ in 2012, 0.02 and 0.03 mmol $Si \cdot m^{-2} \cdot day^{-1}$ in 2014, and 0.11 and 0.12 mmol $Si \cdot m^{-2} \cdot day^{-1}$ in 2016. Overall, the highest value of $bSiO_2$ export (2.82 mmol $Si \cdot m^{-2} \cdot day^{-1}$) was estimated for 0–500 m at Cycle 4 in 2011.

4. Discussion

4.1. Giant Phaeodarian $bSiO_2$ Export From the Euphotic Zone

Our sediment trap deployments conducted between 2011 and 2016 showed that two families of giant phaeodarians, Aulosphaeridae and Castanellidae, contribute an overall average of 10% of $bSiO_2$ export from the euphotic zone but represent a much larger percentage of $bSiO_2$ export in more oligotrophic regions where total export is low. In regions of lowest $bSiO_2$ export, contributions of these two families alone are 10–80% of the flux, declining to 0.1–2% of the flux in waters with the highest $bSiO_2$ export in our region. These highest $bSiO_2$ fluxes are thought be associated with vertical export of diatom frustules (Krause et al., 2015), such as in 2011 (e.g., Cycle 3) where there was iron limitation of diatom growth, sustained uptake of Si, and subsequent high $bSiO_2$ export (Brzezinski et al., 2015). The pattern of increasing contribution with decreasing total $bSiO_2$ flux is consistent for three of our four cruises. However, this relationship differed in 2014 where we documented low phaeodarian standing stocks, reduced phaeodarian vertical fluxes, and consistent contribution to $bSiO_2$ export. In 2014, the CCE was affected by pronounced warm water anomalies (cf. Bond et al., 2015), leading to decreased primary production in our data and throughout the area (Leising et al., 2015). As phaeodarians are known to be flux-feeders (Gowing, 1989), decreased primary production would be expected to be associated with decreased fluxes of particles and reduced food supply. In contrast, during the El Niño spring of 2016, nearshore primary production was comparable to other years (Figure 2c), further underscoring the anomalous perturbations to the ecosystem in summer 2014. Overall, our estimates exceed the range of limited previous results regarding the contribution of phaeodarians to total $bSiO_2$ export (2–23% at the PARFLUX station; Takahashi et al., 1983). The significant contribution of giant phaeodarians is not unexpected as they have been shown to dominate zooplankton biomass in the CCE region (Biard et al., 2016). However, given their ubiquity and broad vertical distribution in the global ocean, it raises the question of their absence in past studies of siliceous rhizarian fluxes.

The present sediment trap fluxes report one of the few assessments of cell-specific vertical fluxes of Aulosphaeridae and Castanellidae. Prior studies have reported vertical fluxes of siliceous rhizarians in multiple locations including the following: the Southern Ocean (Abelmann, 1992), Atlantic Ocean (Boltovskoy et al., 1993a; Michaels et al., 1995; Takahashi & Honjo, 1981), Arctic Ocean (Ikenoue et al., 2012), and Pacific Ocean (Bernstein et al., 1990; Gowing, 1986, 1993; Gowing & Coale, 1989; Takahashi, 1987). There, phaeodarians usually represented a small fraction (~22% on average) of the vertical fluxes of siliceous rhizarians (mainly driven by polycystines; data summarized in Boltovskoy et al., 1993a). Of all these studies, only a handful reported the presence in sediment traps of Castanellidae (Ikenoue et al., 2012; Okazaki et al., 2005; Takahashi, 1987, 1991) and even fewer the presence of Aulosphaeridae along with Castanellidae (Takahashi, 1991, 1997). Vertical fluxes of Castanellidae were similar compared to our mean estimates: 2–318 ind $\cdot m^{-2} \cdot day^{-1}$ compared to 192, but negligible for the Aulosphaeridae: 2–108 ind $\cdot m^{-2} \cdot day^{-1}$ compared to 456 (Takahashi, 1991). These differences could be explained by temporal variability or distinct regional ecological preferences of these phaeodarians but is more likely to result from methodological differences.

Phaeodarians and siliceous rhizarians have cell sizes ranging from tens of micrometers to several centimeters (Ling & Haddock, 1997; Nakamura & Suzuki, 2015; Suzuki & Not, 2015; Swanberg et al., 1986; Takahashi, 1987). In most previous sediment trap studies, the mesh size for counts was 40 μm (Boltovskoy et al., 1993b) and larger organisms were usually discarded (e.g., >100 μm in Gowing, 1993, and >1,000 μm in Takahashi & Honjo, 1981). Given the wide distribution of Castanellidae (Kling, 1976; Tibbs & Tibbs, 1986) and Aulosphaeridae (Biard et al., 2016), it is likely that both were underestimated due to the size selectivity of the previous studies. Additionally, some phaeodarian taxa (e.g., Aulosphaeridae) were consistently absent from sediment trap material, while commonly observed in bottle or net samples (Takahashi, 1981), probably due to the susceptibility of these phaeodarians to rapid dissolution in sediment traps (Erez et al., 1982; Takahashi & Hurd, 2007). Therefore, long deployment times likely favor partial dissolution of the most fragile phaeodarians, leading to underestimations of their vertical fluxes and contribution to $bSiO_2$ export. Unlike most studies of radiolarian fluxes using long deployments of sediment traps (mean = 42 days, range = 1–268; Boltovskoy et al., 1993a), deployment time in the present study averaged three days, and never exceeded six. Phaeodaria were also enumerated within 24 hr of sediment trap recovery, thus likely maximizing the preservation of Aulosphaeridae and Castanellidae.

4.2. Insights From In Situ Measurements of $bSiO_2$ Export in the Mesopelagic

The euphotic zone is typically considered the main locus of $bSiO_2$ production in the ocean and hence main source for vertical flux through mesopelagic waters (Nelson et al., 1995; Tréguer & De La Rocha, 2013). Accordingly, on our cruises, the sampling design focused on quantifying vertical fluxes out of and slightly beneath the euphotic zone. Similar approaches have been used at the BATS site (Nelson & Brzezinski, 1997) or station ALOHA (Brzezinski et al., 2011). Here we show that a significant fraction of total $bSiO_2$ export is derived from phaeodarian production well below the sunlit waters. Across four cruises, in situ estimates of Aulosphaeridae $bSiO_2$ export showed systematic increases when including the mesopelagic. This increase of $bSiO_2$ export with depth is in stark contrast with carbon fluxes in the CCE, which show a mean 27% decrease over a 50 m increase in depth (Stukel et al., 2015). The increase of $bSiO_2$ export with depth is explained by the vertical distribution of Aulosphaeridae, whose abundance maxima are between 100 and 200 m in the CCE and regularly deeper in other regions (Steinberg et al., 2008; Zasko & Rusanov, 2005). In these conditions, sediment trap deployments at the base of the euphotic zone are likely to capture only 33 to 84% of Aulosphaeridae $bSiO_2$ export down to the mesopelagic. Recently, an increase of $bSiO_2$ fluxes with depth has been reported from the PAP site in the Northeast Atlantic Ocean (Giering et al., 2017). Although this pattern was attributed by the authors to an invalid steady state assumption, the present data suggest that it could relate more to the deeper vertical distributions of phaeodarians.

Whether deeper distributions also apply to the Castanellidae $bSiO_2$ export is still unclear, as none of our ~15,000 UVP5 images could be identified as Castanellidae due to a lower size limit of the UVP5 (~600 μm; Biard et al., 2016) that is larger than most of Castanellidae (500–700 μm). Analysis of the Castanellidae community from the eastern Pacific revealed that they were more abundant in the 50–100 m layer (Zasko & Rusanov, 2005). Unlike the Aulosphaeridae, such observations could suggest that our deepest sediment traps (150 m) might have captured most of the Castanellidae-related fluxes in the CCE. However, many species of Castanellidae have been encountered elsewhere in deeper water (>1,000 m) and could represent a

significant fraction of the $bSiO_2$ export below the euphotic zone (Reshetnyak, 1966). Better assessment of the potential deep distributions and fluxes of Castanellidae is required in order to fully appreciate their significance in $bSiO_2$ export.

In the past, in situ imagery has been used for quantification of plankton standing stocks (e.g., Biard et al., 2016; Dennett et al., 2002; Stemmann et al., 2008). To a lesser extent, it has also been used to estimate particles fluxes (e.g., Guidi et al., 2016) with the assumption that particle size distributions can be converted to mass fluxes (Guidi et al., 2008). Here instantaneous $bSiO_2$ export profiles were estimated using parallel deployments between sediment traps and the UVP. In order to use only the UVP, or similar in situ devices, to derive $bSiO_2$ export in the future, several variables need to be known. These include sinking speed of siliceous rhizarians and the actual proportion of sinking organisms (i.e., the sinking population).

Here the inferred sinking speed of the bulk Aulosphaeridae community averaged 23 m/day. However, this bulk sinking speed is unlikely to reflect the actual settling rates of sinking Aulosphaeridae caught in our sediment traps. Rather, it includes a large portion of the community that is healthy and has negligible sinking speeds, combined with a (likely smaller) fraction of the Aulosphaeridae detected by the UVP5 that is either dead or unhealthy, hence sinking much faster. Other studies have determined sinking speeds ranging from 13 to 500 m/day for a wide spectrum of siliceous rhizarians (Berger, 1976; Takahashi & Honjo, 1983). Originally considered as a function of size, sinking speed was later correlated with skeleton mass (Takahashi & Honjo, 1983). We could estimate a typical mass for Aulosphaeridae, and consequently a sinking speed, from *Haeckeliana porcellana*, the closest species to our Aulosphaeridae in terms of silica content. According to Takahashi (1981), this species can sink up to 416 m/day. Therefore, the sinking speed of Aulosphaeridae may be an order of magnitude faster than the overall community rate of 23 m/day estimated here. Expressed differently, this contrast in rates implies that perhaps ~10% of the community was composed of sinking cells. However, with the very limited knowledge of phaeodarian life cycles (Nakamura & Suzuki, 2015) and the lack of data on their mortality rate, we cannot determine rates of production of dead sinking specimens. As it is currently impossible to separate live specimens from dead ones using UVP5 images, direct measures of the ratio between live/dead specimens (e.g., using nuclear staining; Gowing, 1986; or vital dyes) are required to convert standing stock into the actual sinking population. This is an important area deserving future research in order to allow determination of instantaneous fluxes from in situ standing stocks.

4.3. Quantifying the Silica Content of Rhizaria

The silica content of several phaeodarian and nassellarian species was successfully determined from single cells and revealed values among the largest recorded for any siliceous planktonic organism (43.42 μg Si/cell for the colonial phaeodarian *Nationaletta valvidiae*). Higher silica contents (57.9–64 μg Si/cell) have been reported for three phaeodarian species of the genus *Tuscaretta* (Bernstein et al., 1990). However, as mentioned by the authors themselves, these values might have been inflated due to the presence of contaminants (inorganic/organic matter). In comparison with other siliceous plankton, *Ethmodiscus* spp. (mean biovolume = 2.2×10^9 μm^3) has the highest silica content reported for any diatom, averaging 14.1 ± 1.3 μg Si/cell (Villareal et al., 1999). While mostly based on larger specimens, our silica content values are consistent with previous estimates for other siliceous rhizarians (Takahashi, 1981), allowing for differences in cell size.

Measurements of silica content revealed important intraspecific variability in most taxa. Although we used care in cleaning specimens, the very delicate nature of phaeodarian skeletons (Nakamura & Suzuki, 2015) could have led to damage prior to and/or following collection and cleaning procedures, leading to inflated variability in silica content. Along with 23 literature values (Takahashi, 1981), six specimens were collected from sediment traps, but we did not observe a significant difference with the silica content of live specimens. Yet due to the labile nature of the phaeodarian skeleton and their susceptibility to dissolution (Erez et al., 1982; Takahashi & Hurd, 2007), we cannot exclude the possibility of partially dissolved skeletons in the literature values. Also, as some fragile taxa such as the Aulacanthidae may be undersampled in sediment traps due to dissolution biases (Takahashi, 1981), we recommend the use of fresh plankton specimens in future studies.

This is the first report of allometric relationships specific to phaeodarians. Similar relationships have been reported for both marine and freshwater diatoms (Conley et al., 1989), and subsequently used to determine silica contents for marine silicoflagellates (Takahashi, 1989). Interestingly, we showed that silica content is

Table 2
Estimated Regional Contribution of the Giant Phaeodarian Aulosphaeridae to Total $bSiO_2$ Export

Biome	Type	$bSiO_2$ fluxes from the euphotic zone (mmol Si · m^{-2} · day^{-1})			UVP5 Aulosphaeridae $bSiO_2$ fluxes at 0–150 m (μmol Si · m^{-2} · day^{-1})		Median contribution (95% CI) [range] (%)	Deep $bSiO_2$ flux[a] (mmol Si · m^{-2} · day^{-1})		UVP5 Aulosphaeridae $bSiO_2$ fluxes at 0–500 m (μmol Si · m^{-2} · day^{-1})		Median contribution (95% CI) [range] (%)
		Depth (m)	Range (min-max)	Mean	Range (min-max)	Median (95% CI)		Range (min-max)	Mean	Range (min-max)	Median (95% CI)	
Antarctic Biome	Oceanic	50–100	0.88–6.03[b]	2.63[b]	0–15	0 (0)	0 (0) [0–0.57]	0.01–2.51	0.78	0–64	15 (10–23)	1.91 (1.38–2.97) [0–8.18]
Atlantic Polar Biome	Oceanic	20–200	0.12–9.19[c]	3.99[c]	0–29	0 (0)	0 (0) [0–0.73]	0.004–0.22	0.08	0–67	0 (0)	0 (0) [0–84]
California Upwelling Coastal	Coastal	50–150	0.001–20.32	3.77	0–2389	121 (88–189)	3.21 (2.33–5.01) [0–63]	0.15–2.18	0.76	0–2815	195 (141–303)	26 (19–40) [0–370]
Indian Ocean Trade Wind Biome	Coastal	100	–	0.95[d]	0–63	0.47 (0.34–0.72)	0.05 (0.04–0.08) [0–7]	–	0.47	0–63	5.14 (3.72–799)	1.09 (0.79–1.7) [0–13]
	Oceanic	100	0.23–1.51[d]	0.91[d]	0-7	0 (0)	0 (0) [0–0.77]	0.12–0.76	0.45	0–23	0 (0)	0 (0) [0–5.05]
Mediterranean Sea	Oceanic	100	0.29–0.32[d]	0.31[d]	0-35	0 (0)	0 (0) [0–11]	0.15–0.16	0.15	0–29	0 (0)	0 (0) [0–20]
Atlantic Westerly Winds Biome	Coastal	–	–	–	0–1	0 (0)	-	–	–	0–4.31	0 (0)	-
	Oceanic	150	0.017–0.7[e]	0.098[d]	0-15	0 (0)	0 (0) [0–15]	0.02–0.36	0.12	0–54	0 (0)	0 (0) [0–45]
Pacific Trade Wind Biome	Coastal	100	0.002–3.82[d]	1.38[f]	0-28	3.12 (2.26–4.86)	0.23 (0.16–0.35) [0–2.03]	0.001–1.91	0.69	0–291	24 (17–37)	3.44 (2.49–5.35) [0–42]
	Oceanic	150	0.014–0.3[f]	0.09[f]	0-777	0 (0)	0 (0) [0–863]	0.02–0.13[g]	0.04[g]	0-852	4.32 (3.13–6.72)	11 (7.82–17) [0–2131]
Atlantic Trade Wind Biome	Coastal	–	–	–	0–8	0 (0)	-	–	–	0–20	0 (0)	-
	Oceanic	100	0.29–0.75[d]	0.52[d]	0-17	0 (0)	0 (0) [0–3.27]	0.03–0.38	0.13	0–81	2.11 (1.53–3.29)	1.63 (1.18–2.53) [0–63]

[a]If not specified otherwise, $bSiO_2$ export values at 2,000 m from Honjo et al. (2008) and references therein. [b]Daily estimates from a range of annual rates among Southern Ocean zones (Nelson et al., 2002, and references therein). [c]Krause unpubl. [d]Daily estimates computed from annual ranges of $bSiO_2$ export at 2,000 m (Honjo et al., 2008, and references therein) and assuming 50% dissolution between the euphotic zone base and 2,000 m. [e]Brzezinski et al. (2011) and references therein. [f]Brzezinski et al. (2011). [g]$bSiO_2$ export at 4,000 m (Karl et al., 2012).

also related to cell length and biovolume when considering together 31 siliceous rhizarian taxa from four groups. While the skeletal morphology of Phaeodaria differs radically from that of polycystine radiolarians, the former displaying hollow structures (Nakamura & Suzuki, 2015) and the latter solid "plain" structures (Suzuki & Not, 2015), this relationship highlights a similarity in skeletal composition between two genetically distinct rhizarian groups (Cercozoa and Retaria). However, with an imbalance of specimen number between phaeodarians and polycystine radiolarians, 70 and 18, respectively, additional measurements of silica content are needed to confirm the validity of this relationship. Nevertheless, these new silica content relationships provide the most robust tool available thus far for incorporating siliceous rhizarians in silica budgets at local-to-global scales.

4.4. Potential Significance of Giant Phaeodarians and Siliceous Rhizarians in the Global Silica Cycle

Given their new-found importance to carbon cycling and plankton biomass (Biard et al., 2016; Guidi et al., 2016), Rhizaria, and specifically Phaeodaria, potentially play a significant role in global oceanic silica fluxes. In one of the latest reviews of the global silica budget, Tréguer and De La Rocha (2013) proposed that radiolarians could contribute between 0.001 and 6 mmol/m^2 of $bSiO_2$ standing stocks in the euphotic zone (120 m). In order to address the importance of giant phaeodarians to $bSiO_2$ export, we now use a data set of worldwide in situ vertical profiles (Biard et al., 2016). Using the allometry between silica content and biovolume (equation (2)), we estimate Aulosphaeridae $bSiO_2$ standing stocks (0–150 m) to range from <0.01 to 10 mmol Si/m^2. When considering standing stocks integrated down to mesopelagic waters (0–500 m), values increase to 12 mmol Si/m^2. However, the present range of values represents only a single family, the Aulosphaeridae. Other giants, such as the colonial Collodaria, can also be found at high densities, especially in the most oligotrophic regions (Biard et al., 2016). Since about two thirds of these colonial collodarians are siliceous (Biard et al., 2017), they are likely to represent a substantial pool of $bSiO_2$ in the oligotrophic gyres. If the range of rhizarian $bSiO_2$ standing stock proposed by Tréguer and De La Rocha (2013) is a good approximation for the smaller size fractions of siliceous rhizarians, adding the contribution of siliceous giants, such as the Aulosphaeridae or the colonial Collodaria, provides a rhizarian $bSiO_2$ standing stock in the euphotic zone much larger than previously expected. With total $bSiO_2$ standing stocks in the upper 120 m of the oligotrophic and HNLC regions of the ocean ranging between 2 and 26 mmol Si/m^2 (Adjou et al., 2011, and references therein), an estimated contribution of the entire size spectrum of siliceous Rhizaria, ranging from 0.5 to 16 mmol Si/m^2, suggests that they could represent more than a third of this standing stock in those regions. If valid worldwide, this assumption would corroborate an early study suggesting that radiolarians (probably including phaeodarians) are the second most important producers of suspended silica in the ocean after diatoms (Lisitzin, 1972).

Our results show that in addition to their significance as silica producers, giant phaeodarians are also important vectors of $bSiO_2$ export. Assuming that our effective sinking speed (23 m/day) is representative of several trophic conditions, from eutrophic coastal zones to offshore oligotrophic regions, we estimated the amount of $bSiO_2$ exported by Aulosphaeridae worldwide (Table 2). To assess their importance to $bSiO_2$ export from the euphotic zone and to the deep ocean, we compared our estimates to regional assessments (Brzezinski et al., 2011; Krause et al., 2015; Nelson et al.,

2002) and global estimates of deep $bSiO_2$ export (Honjo et al., 2008, and reference herein). Worldwide, Aulosphaeridae $bSiO_2$ export from the euphotic zone could range between 0 and 2.8 mmol $Si \cdot m^{-2} \cdot day^{-1}$. Their contribution appears minimal with the exception of our study region, the CCE, locally exceeding 3% of the euphotic $bSiO_2$ export (median value). For the Aulosphaeridae, the contribution of $bSiO_2$ export at 500 m to deep $bSiO_2$ export (>2 km) appears significantly higher, ranging from 0 to a maximum of 26%. Although their contribution appears modest globally, a few very high percentages were found (Table 2). Whether these high contributions are the result of temporal variability of the phaeodarian community or their known patchiness (Bernstein et al., 1990), locally, Aulosphaeridae could have a significant impact in the export of $bSiO_2$ to the deep ocean.

Despite the uncertainties associated with such global estimates, the paucity of sampling stations, and our limited knowledge of siliceous rhizarian ecology (Suzuki & Not, 2015), these estimates of $bSiO_2$ standing stock and export should be considered a first attempt to assess their global significance in the marine silica cycle. As these values mainly recognize the role of one single phaeodarian family (Aulosphaeridae), our estimates should be considered as minimal values. Together with the already suggested importance of smaller radiolarians in $bSiO_2$ production (Lisitzin, 1972; Takahashi et al., 1983), inclusion of these giants should considerably increase the importance of siliceous rhizarians globally. Additionally, the increased contribution of Phaeodaria to $bSiO_2$ export in regions of low $bSiO_2$ export has broader implications when considering $bSiO_2$ export at the global scale. Regions of high $bSiO_2$ export are usually encountered near the Southern Ocean, the Subarctic Pacific, or in coastal regions, while regions of low export are found in oligotrophic gyres (Lisitzin, 1972; Pichevin et al., 2014). These gyres are among the largest ecosystems on Earth, representing nearly 40% of the planet's surface, and appear to be increasing in spatial extent (Polovina et al., 2008). With the recent observation of large biomasses of phaeodarians in the oligotrophic ocean (Biard et al., 2016), the significance of phaeodarians and siliceous rhizarians may have been overlooked in these regions, especially given their vertical maxima in mesopelagic waters. If valid globally, this observation might substantially change understanding of silica dynamics in the oligotrophic oceans and previous interpretations of $bSiO_2$ fluxes as a specific metric for diatom export. Along with additional measures of rhizarians' silica content, better estimates of their vertical fluxes across a wider range of cell sizes, uptake rates of silicic acid, accurate estimates of their sinking velocity, and differentiation of living and dead cells are required in order to better appreciate the global significance of siliceous rhizarians and ultimately include this emerging component of the marine silica cycle into biogeochemical models.

Acknowledgments
This work was supported by the Scripps Postdoctoral Fellowship program, National Science Foundation grants OCE-1637632 and OCE-1614359 to the CCE-LTER site, and internal support from the Dauphin Island Sea Lab. We thank to Y. Nakamura and N. Suzuki for their help with the taxonomic outline of Rhizaria and the anonymous referees for their constructive comments. We are grateful to M. Picheral for his help handling the UVP5 data and the operators who conducted UVP5 deployments during the four process cruises. Thanks to S. Acton and E. Lachenmeyer for laboratory assistance. Data used in this manuscript are publicly available on the CCE-LTER Datazoo website (http://oceaninformatics.ucsd.edu/datazoo/catalogs/ccelter/datasets).This study is a contribution from the CHAIRE Vision, supported by the CNRS and Sorbonne University and the French Investissements d'Avenir program.

References

Abelmann, A. (1992). Radiolarian flux in Antarctic waters (drake passage, Powell Basin, Bransfield Strait). *Polar Biology*, *12*(3–4), 357–372. https://doi.org/10.1007/BF00243107

Adjou, M., Tréguer, P., Dumousseaud, C., Corvaisier, R., Brzezinski, M. A., & Nelson, D. M. (2011). Particulate silica and Si recycling in the surface waters of the eastern equatorial Pacific. *Deep Sea Research Part II: Topical Studies in Oceanography*, *58*(3-4), 449–461. https://doi.org/10.1016/j.dsr2.2010.08.002

Baines, S. B., Twining, B. S., Brzezinski, M. A., Krause, J. W., Vogt, S., Assael, D., & McDaniel, H. (2012). Significant silicon accumulation by marine picocyanobacteria. *Nature Geoscience*, *5*(12), 886–891. https://doi.org/10.1038/ngeo1641

Berger, W. H. (1976). Biogenous Deep Sea sediments: Production, preservation and interpretation. In J. P. Riley & R. Chester (Eds.), *Chemical Oceanography* (Vol. 5, pp. 265–388). London: Academic Press.

Bernstein, R. E., Betzer, P. R., & Takahashi, K. (1990). Radiolarians from the western North Pacific Ocean: A latitudinal study of their distributions and fluxes. *Deep Sea Research Part A. Oceanographic Research Papers*, *37*(11), 1677–1696. https://doi.org/10.1016/0198-0149(90)90071-3

Biard, T., Bigeard, E., Audic, S., Poulain, J., Gutierrez-Rodriguez, A., Pesant, S., et al. (2017). Biogeography and diversity of Collodaria (Radiolaria) in the global ocean. *The ISME Journal*, *11*(6), 1331–1344. https://doi.org/10.1038/ismej.2017.12

Biard, T., Stemmann, L., Picheral, M., Mayot, N., Vandromme, P., Hauss, H., et al. (2016). In situ imaging reveals the biomass of giant protists in the global ocean. *Nature*, *532*(7600), 504–507. https://doi.org/10.1038/nature17652

Boltovskoy, D., Alder, V. A., & Abelmann, A. (1993a). Annual flux of radiolaria and other shelled plankters in the eastern equatorial Atlantic at 853 m: Seasonal variations and polycystine species-specific responses. *Deep Sea Research Part I: Oceanographic Research Papers*, *40*(9), 1863–1895. https://doi.org/10.1016/0967-0637(93)90036-3

Boltovskoy, D., Alder, V. A., & Abelmann, A. (1993b). Radiolarian sedimentary imprint in Atlantic equatorial sediments: Comparison with the yearly flux at 853 m. *Marine Micropaleontology*, *23*(1), 1–12. https://doi.org/10.1016/0377-8398(93)90051-X

Bond, N. A., Cronin, M. F., Freeland, H., & Mantua, N. (2015). Causes and impacts of the 2014 warm anomaly in the NE Pacific. *Geophysical Research Letters*, *42*, 3414–3420. https://doi.org/10.1002/2015GL063306

Brzezinski, M. A., Krause, J. W., Bundy, R. M., Barbeau, K. A., Franks, P., Goericke, R., et al. (2015). Enhanced silica ballasting from iron stress sustains carbon export in a frontal zone within the California current. *Journal of Geophysical Research: Oceans*, *120*, 4654–4669. https://doi.org/10.1002/2015JC010829

Brzezinski, M. A., Krause, J. W., Church, M. J., Karl, D. M., Li, B., Jones, J. L., & Updyke, B. (2011). The annual silica cycle of the North Pacific subtropical gyre. *Deep Sea Research Part I: Oceanographic Research Papers*, *58*(10), 988–1001. https://doi.org/10.1016/j.dsr.2011.08.001

Burki, F., & Keeling, P. J. (2014). Rhizaria. *Current Biology*, *24*(3), R103–R107. https://doi.org/10.1016/j.cub.2013.12.025

Conley, D. J., Kilham, S. S., & Theriot, E. (1989). Differences in silica content between marine and freshwater diatoms. *Limnology and Oceanography*, *34*(1), 205–212. https://doi.org/10.4319/lo.1989.34.1.0205

De Wever, P., Dumitrica, P., Caulet, J. P., Nigrini, C., & Caridroit, M. (2002). *Radiolarians in the Sedimentary Record* (p. 533). London: CRC Press.

Dennett, M. R., Caron, D. A., Michaels, A. F., Gallager, S. M., & Davis, C. S. (2002). Video plankton recorder reveals high abundances of colonial Radiolaria in surface waters of the central North Pacific. *Journal of Plankton Research*, *24*(8), 797–805. https://doi.org/10.1093/plankt/24.8.797

Ducklow, H., Steinberg, D., & Buesseler, K. (2001). Upper Ocean carbon export and the biological pump. *Oceanography*, *14*(4), 50–58. https://doi.org/10.5670/oceanog.2001.06

Dumitrica, P., & Van Eetvelde, Y. (2009). Late Paleocene Phaeodaria (Radiolaria) from Denmark. *Revue de Micropaleontologie*, *52*(3), 219–226. https://doi.org/10.1016/j.revmic.2008.04.001

Eppley, R. W., & Peterson, B. J. (1979). Particulate organic matter flux and planktonic new production in the deep ocean. *Nature*, *282*(5740), 677–680. https://doi.org/10.1038/282677a0

Erez, J., Takahashi, K., & Honjo, S. (1982). In-situ dissolution experiment of radiolaria in the central North Pacific Ocean. *Earth and Planetary Science Letters*, *59*(2), 245–254. https://doi.org/10.1016/0012-821X(82)90129-7

Falkowski, P. G., Barber, R. T., & Smetacek, V. (1998). Biogeochemical controls and feedbacks on ocean primary production. *Science*, *281*(5374), 200–206. https://doi.org/10.1126/science.281.5374.200

Giering, S. L. C., Sanders, R., Martin, A. P., Henson, S. A., Riley, J. S., Marsay, C. M., & Johns, D. G. (2017). Particle flux in the oceans: Challenging the steady state assumption. *Global Biogeochemical Cycles*, *31*, 159–171. https://doi.org/10.1002/2016GB005424

Goericke, R. (2017). Primary Production Estimates from 14C Uptake (In Situ), Determined by the Incorporation of Inorganic Carbon into Particulate Organic Carbon (POC) Due to Photosynthesis at Selected Light Levels from CCE LTER Process Cruises in the California Current System, 2006–2016 (Ongoing). *Environmental Data Initiative*. https://doi.org/10.6073/pasta/5904efd7c22718ce64408238d446cd74

Gorsky, G., Ohman, M. D., Picheral, M., Gasparini, S., Stemmann, L., Romagnan, J.-B., et al. (2010). Digital zooplankton image analysis using the ZooScan integrated system. *Journal of Plankton Research*, *32*(3), 285–303. https://doi.org/10.1093/plankt/fbp124

Gowing, M. M. (1986). Trophic biology of phaeodarian radiolarians and flux of living radiolarians in the upper 2000 m of the North Pacific central gyre. *Deep Sea Research Part A. Oceanographic Research Papers*, *33*(5), 655–674. https://doi.org/10.1016/0198-0149(86)90059-2

Gowing, M. M. (1989). Abundance and feeding ecology of Antarctic phaeodarian radiolarians. *Marine Biology*, *103*(1), 107–118. https://doi.org/10.1007/BF00391069

Gowing, M. M. (1993). Seasonal radiolarian flux at the VERTEX North Pacific time-series site. *Deep Sea Research Part I: Oceanographic Research Papers*, *40*(3), 517–545. https://doi.org/10.1016/0967-0637(93)90144-R

Gowing, M. M., & Coale, S. L. (1989). Fluxes of living radiolarians and their skeletons along a Northeast Pacific transect from coastal upwelling to open ocean waters. *Deep Sea Research Part A. Oceanographic Research Papers*, *36*(4), 561–576. https://doi.org/10.1016/0198-0149(89)90006-X

Guidi, L., Chaffron, S., Bittner, L., Eveillard, D., Larhlimi, A., Roux, S., et al. (2016). Plankton networks driving carbon export in the oligotrophic ocean. *Nature*, *532*(7600), 465–470. https://doi.org/10.1038/nature16942

Guidi, L., Jackson, G. A., Stemmann, L., Miquel, J. C., Picheral, M., & Gorsky, G. (2008). Relationship between particle size distribution and flux in the mesopelagic zone. *Deep Sea Research Part I: Oceanographic Research Papers*, *55*(10), 1364–1374. https://doi.org/10.1016/j.dsr.2008.05.014

Hamm, C., & Smetacek, V. (2007). Armor: Why, when and how. In P. G. Falkowski & A. H. Knoll (Eds.), *Evolution of Primary Producers in the Sea*, (pp. 311–332). Amsterdam, Netherlands: Elsevier. https://doi.org/10.1016/B978-012370518-1/50015-1

Honjo, S., Manganini, S. J., Krishfield, R. A., & Francois, R. (2008). Particulate organic carbon fluxes to the ocean interior and factors controlling the biological pump: A synthesis of global sediment trap programs since 1983. *Progress in Oceanography*, *76*(3), 217–285. https://doi.org/10.1016/j.pocean.2007.11.003

Ikenoue, T., Takahashi, K., & Tanaka, S. (2012). Fifteen year time-series of radiolarian fluxes and environmental conditions in the Bering Sea and the central subarctic Pacific, 1990–2005. *Deep Sea Research Part II: Topical Studies in Oceanography*, *61-64*, 17–49. https://doi.org/10.1016/j.dsr2.2011.12.003

Jacox, M. G., Hazen, E. L., Zaba, K. D., Rudnick, D. L., Edwards, C. A., Moore, A. M., & Bograd, S. J. (2016). Impacts of the 2015–2016 El Niño on the California current system: Early assessment and comparison to past events. *Geophysical Research Letters*, *43*, 7072–7080. https://doi.org/10.1002/2016GL069716

Karl, D. M., Church, M. J., Dore, J. E., Letelier, R. M., & Mahaffey, C. (2012). Predictable and efficient carbon sequestration in the North Pacific Ocean supported by symbiotic nitrogen fixation. *Proceedings of the National Academy of Sciences of the United States of America*, *109*(6), 1842–1849. https://doi.org/10.1073/pnas.1120312109

Kling, S. A. (1976). Relation of radiolarian distributions to subsurface hydrography in the North Pacific. *Deep Sea Research and Oceanographic Abstracts*, *23*(11), 1043–1058. https://doi.org/10.1016/0011-7471(76)90880-9

Knauer, G. A., Martin, J. H., & Bruland, K. W. (1979). Fluxes of particulate carbon, nitrogen, and phosphorus in the upper water column of the Northeast Pacific. *Deep Sea Research Part A. Oceanographic Research Papers*, *26*(1), 97–108. https://doi.org/10.1016/0198-0149(79)90089-X

Krause, J. W., Brzezinski, M. A., Baines, S. B., Collier, J. L., Twining, B. S., & Ohnemus, D. C. (2017). Picoplankton contribution to biogenic silica stocks and production rates in the Sargasso Sea. *Global Biogeochemical Cycles*, *31*, 762–774. https://doi.org/10.1002/2017GB005619

Krause, J. W., Brzezinski, M. A., Goericke, R., Landry, M. R., Ohman, M. D., Stukel, M. R., & Taylor, A. G. (2015). Variability in diatom contributions to biomass, organic matter production and export across a frontal gradient in the California current ecosystem. *Journal of Geophysical Research: Oceans*, *120*, 1032–1047. https://doi.org/10.1002/2014JC010472

Landry, M. R., Ohman, M. D., Goericke, R., Stukel, M. R., & Tsyrklevich, K. (2009). Lagrangian studies of phytoplankton growth and grazing relationships in a coastal upwelling ecosystem off Southern California. *Progress in Oceanography*, *83*(1-4), 208–216. https://doi.org/10.1016/j.pocean.2009.07.026

Legendre, P. (2014). lmodel2: Model II regression (Version 1.7.2). Retrieved from https://cran.r-project.org/web/packages/lmodel2/index.html

Leising, A. W., Schroeder, I. D., Bograd, S. J., Abell, J., Durazo, R., et al. (2015). State of the California Current 2014–15: Impacts of the Warm-Water "Blob". *California Cooperative Oceanic Fisheries Investigations Reports*, *56*, 31–68.

Ling, H. Y., & Haddock, S. H. D. (1997). The enclosing latticed sphere of Tuscaridium cygneum (Murray), a eurybathyal phaeodarian Radiolaria, from the North Pacific. *Paleontological Research*, *1*(2), 144–149. https://doi.org/10.2517/prpsj.1.144

Lisitzin, A. P. (1972). Sedimentation in the world ocean. *Society of Economic Paleontologists and Mineralogists*, *17*, 218–241.

Matsuzaki, K. M., Suzuki, N., & Nishi, H. (2015). Middle to upper Pleistocene polycystine radiolarians from hole 902-C9001C, northwestern Pacific. *Paleontological Research*, *19*(s1), 1–77. https://doi.org/doi:10.2517/2015PR003

Michaels, A. F., Caron, D. A., Swanberg, N. R., Howse, F. A., & Michaels, C. M. (1995). Planktonic sarcodines (Acantharia, Radiolaria, foraminifera) in surface waters near Bermuda: Abundance, biomass and vertical flux. *Journal of Plankton Research*, *17*(1), 131–163. https://doi.org/10.1093/plankt/17.1.131

Mortlock, R. A., & Froelich, P. N. (1989). A simple method for the rapid determination of biogenic opal in pelagic marine sediments. *Deep Sea Research Part A. Oceanographic Research Papers*, *36*(9), 1415–1426. https://doi.org/10.1016/0198-0149(89)90092-7

Nakamura, Y., Imai, I., Yamaguchi, A., Tuji, A., Not, F., & Suzuki, N. (2015). Molecular phylogeny of the widely distributed marine Protists, Phaeodaria (Rhizaria, Cercozoa). *Protist*, *166*(3), 363–373. https://doi.org/10.1016/j.protis.2015.05.004

Nakamura, Y., & Suzuki, N. (2015). Phaeodaria: Diverse marine Cercozoans of world-wide distribution. In S. Ohtsuka, T. Suzaki, T. Horiguchi, N. Suzuki, & F. Not (Eds.), *Marine Protists* (pp. 223–249). Tokyo, Japan: Springer.

Nelson, D. M., Anderson, R. F., Barber, R. T., Brzezinski, M. A., Buesseler, K. O., Chase, Z., et al. (2002). Vertical budgets for organic carbon and biogenic silica in the Pacific sector of the Southern Ocean, 1996–1998. *Deep Sea Research Part II: Topical Studies in Oceanography*, *49*(9-10), 1645–1674. https://doi.org/10.1016/S0967-0645(02)00005-X

Nelson, D. M., & Brzezinski, M. A. (1997). Diatom growth and productivity in an oligo-trophic midocean gyre: A 3-yr record from the Sargasso Sea near Bermuda. *Limnology and Oceanography*, *42*(3), 473–486. https://doi.org/10.4319/lo.1997.42.3.0473

Nelson, D. M., Tréguer, P., Brzezinski, M. A., Leynaert, A., & Quéguiner, B. (1995). Production and dissolution of biogenic silica in the ocean: Revised global estimates, comparison with regional data and relationship to biogenic sedimentation. *Global Biogeochemical Cycles*, *9*(3), 359–372. https://doi.org/10.1029/95GB01070

Nikolaev, S. I., Berney, C., Fahrni, J. F., Bolivar, I., Polet, S., Mylnikov, A. P., et al. (2004). The twilight of Heliozoa and rise of Rhizaria, an emerging supergroup of amoeboid eukaryotes. *Proceedings of the National Academy of Sciences of the United States of America*, *101*(21), 8066–8071. https://doi.org/10.1073/pnas.0308602101

Ohman, M., Barbeau, K., Franks, P., Goericke, R., Landry, M., & Miller, A. (2013). Ecological transitions in a coastal upwelling ecosystem. *Oceanography*, *26*(3), 210–219. https://doi.org/10.5670/oceanog.2013.65

Ohman, M. D., Powell, J. R., Picheral, M., & Jensen, D. W. (2012). Mesozooplankton and particulate matter responses to a deep-water frontal system in the southern California current system. *Journal of Plankton Research*, *34*(9), 815–827. https://doi.org/10.1093/plankt/fbs028

Okazaki, Y., Takahashi, K., Onodera, J., & Honda, M. C. (2005). Temporal and spatial flux changes of radiolarians in the northwestern Pacific Ocean during 1997–2000. *Deep Sea Research Part II: Topical Studies in Oceanography*, *52*(16-18), 2240–2274. https://doi.org/10.1016/j.dsr2.2005.07.006

Pena, E. A., & Slate, E. H. (2014). gvlma: Global Validation of Linear Models Assumptions (Version 1.0.0.2). Retrieved from https://cran.r-project.org/web/packages/gvlma/index.html

Picheral, M. (2017). EcoTaxa, a tool for the taxonomic classification of images (Version 1.3). Retrieved from http://ecotaxa.obs-vlfr.fr

Picheral, M., Guidi, L., Stemmann, L., Karl, D. M., Iddaoud, G., & Gorsky, G. (2010). The underwater vision profiler 5: An advanced instrument for high spatial resolution studies of particle size spectra and zooplankton. *Limnology and Oceanography: Methods*, *8*(9), 462–473. https://doi.org/10.4319/lom.2010.8.462

Pichevin, L. E., Ganeshram, R. S., Geibert, W., Thunell, R., & Hinton, R. (2014). Silica burial enhanced by iron limitation in oceanic upwelling margins. *Nature Geoscience*, *7*(7), 541–546. https://doi.org/10.1038/ngeo2181

Polet, S., Berney, C., Fahrni, J., & Pawlowski, J. a. n. (2004). Small-subunit ribosomal RNA gene sequences of Phaeodarea challenge the Monophyly of Haeckel's Radiolaria. *Protist*, *155*(1), 53–63. https://doi.org/10.1078/1434461000164

Polovina, J. J., Howell, E. A., & Abecassis, M. (2008). Ocean's least productive waters are expanding. *Geophysical Research Letters*, *35*, L03618. https://doi.org/10.1029/2007GL031745

R Core Team (2017). R: A language and environment for statistical computing. Vienna, Austria: R Foundation for Statistical Computing. Retrieved from https://www.r-project.org/

Ragueneau, O., Tréguer, P., Leynaert, A., Anderson, R. F., Brzezinski, M. A., DeMaster, D. J., et al. (2000). A review of the Si cycle in the modern ocean: recent progress and missing gaps in the application of biogenic opal as a paleoproductivity proxy. *Global and Planetary Change*, *26*(4), 317–365. https://doi.org/10.1016/S0921-8181(00)00052-7

Reshetnyak, V. V. (1966). Deepwater Phaeodarian radiolarians of the northwestern part of the Pacific Ocean. Fauna of the USSR. Radiolaria. *Akademiia nauk SSSR, Zoologicheskiĭ institut*, *94*, 1–208.

Smetacek, V. (2000). Oceanography: The giant diatom dump. *Nature*, *406*(6796), 574–575. https://doi.org/10.1038/35020665

Stadum, C. J., & Ling, H.-Y. (1969). Tripylean Radiolaria in Deep-Sea sediments of the Norwegian Sea. *Micropaleontology*, *15*(4), 481–489. https://doi.org/10.2307/1484895

Steinberg, D. K., Cope, J. S., Wilson, S. E., & Kobari, T. (2008). A comparison of mesopelagic mesozooplankton community structure in the subtropical and subarctic North Pacific Ocean. *Deep Sea Research Part II: Topical Studies in Oceanography*, *55*(14–15), 1615–1635. https://doi.org/10.1016/j.dsr2.2008.04.025

Stemmann, L., Youngbluth, M., Robert, K., Hosia, A., Picheral, M., Paterson, H., et al. (2008). Global zoogeography of fragile macrozooplankton in the upper 100–1000 m inferred from the underwater video profiler. *ICES Journal of Marine Science: Journal Du Conseil*, *65*(3), 433–442. https://doi.org/10.1093/icesjms/fsn010

Stukel, M. R., Aluwihare, L. I., Barbeau, K. A., Chekalyuk, A. M., Goericke, R., Miller, A. J., et al. (2017). Mesoscale Ocean fronts enhance carbon export due to gravitational sinking and subduction. *Proceedings of the National Academy of Sciences of the United States of America*, *114*(6), 1252–1257. https://doi.org/10.1073/pnas.1609435114

Stukel, M. R., Kahru, M., Benitez-Nelson, C. R., Décima, M., Goericke, R., Landry, M. R., & Ohman, M. D. (2015). Using Lagrangian-based process studies to test satellite algorithms of vertical carbon flux in the eastern North Pacific Ocean. *Journal of Geophysical Research: Oceans*, *120*, 7208–7222. https://doi.org/10.1002/2015JC011264

Stukel, M. R., Ohman, M. D., Benitez-Nelson, C. R., & Landry, M. R. (2013). Contributions of mesozooplankton to vertical carbon export in a coastal upwelling system. *Marine Ecology Progress Series*, *491*, 47–65. https://doi.org/10.3354/meps10453

Stumm, W., & Morgan, J. J. (2012). *Aquatic chemistry: Chemical equilibria and rates in natural waters* (3rd ed., p. 1022). New York: John Wiley.

Suzuki, N., & Aita, Y. (2011). Radiolaria: Achievements and unresolved issues: Taxonomy and cytology. *Plankton & Benthos Research*, *6*(2), 69–91. https://doi.org/10.3800/pbr.6.69

Suzuki, N., & Not, F. (2015). Biology and Ecology of Radiolaria. In S. Ohtsuka, T. Suzaki, T. Horiguchi, N. Suzuki, & F. Not (Eds.), *Marine Protists* (pp. 179–222). Tokyo, Japan: Springer.

Swanberg, N., Bennett, P., Lindsey, J. L., & Anderson, O. R. (1986). The biology of a coelodendrid: A mesopelagic phaeodarian radiolarian. *Deep Sea Research Part A. Oceanographic Research Papers*, *33*(1), 15–25. https://doi.org/10.1016/0198-0149(86)90105-6

Takahashi, K. (1981). Vertical Flux, Ecology and Dissolution of Radiolaria in Tropical Oceans: Implications for the Silica Cycle, (Doctoral dissertation). Retrieved from Woods Hole Open Access Server https://darchive.mblwhoilibrary.org/handle/1912/2420 WoodsHoleOceanographicInstitution: Massachusetts Institute of Technology

Takahashi, K. (1987). Radiolarian flux and seasonality: Climatic and El Nino response in the subarctic Pacific, 1982–1984. *Global Biogeochemical Cycles*, *1*(3), 213–231. https://doi.org/10.1029/GB001i003p00213

Takahashi, K. (1989). Silicoflagellates as productivity indicators: Evidence from long temporal and spatial flux variability responding to hydrography in the northeastern Pacific. *Global Biogeochemical Cycles*, *3*(1), 43–61. https://doi.org/10.1029/GB003i001p00043

Takahashi, K. (1991). *Radiolaria: flux, ecology, and taxonomy in the Pacific and Atlantic*, *Ocean Biocoenosis Series* (p. 303). Woods Hole, MA: Woods Hole Oceanographic Institution.

Takahashi, K. (1997). Time-series fluxes of Radiolaria in the eastern subarctic Pacific Ocean. *News of Osaka Micropaleontologists, Special Volume*, *10*, 299–309.

Takahashi, K., & Honjo, S. (1981). Vertical flux of Radiolaria: A taxon-quantitative sediment trap study from the western tropical Atlantic. *Micropaleontology*, *27*(2), 140–190. https://doi.org/10.2307/1485284

Takahashi, K., & Honjo, S. (1983). Radiolarian skeletons: Size, weight, sinking speed, and residence time in tropical pelagic oceans. *Deep Sea Research Part A. Oceanographic Research Papers*, *30*(5), 543–568. https://doi.org/10.1016/0198-0149(83)90088-2

Takahashi, K., & Hurd, D. C. (2007). Micro- and ultra-structures of phaeodarian Radiolaria. *Memoirs of the Faculty of Science, Kyushu University. Series D, Earth and Planetary Sciences*, *31*(4), 137–158.

Takahashi, K., Hurd, D. C., & Honjo, S. (1983). Phaeodarian skeletons: Their role in silica transport to the Deep Sea. *Science*, *222*(4624), 616–618. https://doi.org/10.1126/science.222.4624.616

Tibbs, J. F., & Tibbs, S. D. (1986). Further Studies on the Phaeodaria (Protozoa: Radiolaria) of the Antarctic Seas. In L. S. Kornicker (Ed.), *Biology of the Antarctic Seas XVI* (pp. 167–202). Washington, DC: American Geophysical Union.

Tréguer, P., Nelson, D. M., Bennekom, A. J. V., DeMaster, D. J., Leynaert, A., & Quéguiner, B. (1995). The silica balance in the World Ocean: A Reestimate. *Science*, *268*(5209), 375–379. https://doi.org/10.1126/science.268.5209.375

Tréguer, P. J., & De La Rocha, C. L. (2013). The World Ocean silica cycle. *Annual Review of Marine Science*, *5*(1), 477–501. https://doi.org/10.1146/annurev-marine-121211-172346

Villareal, T. A., Joseph, L., Brzezinski, M. A., Shipe, R. F., Lipschultz, F., & Altabet, M. A. (1999). Biological and chemical characteristics of the Giant diatom Ethmodiscus (bacillariophyceae) in the central North Pacific gyre. *Journal of Phycology*, *35*(5), 896–902. https://doi.org/10.1046/j.1529-8817.1999.3550896.x

Wickham, H., & RStudio (2017). tidyverse: Easily Install and Load 'Tidyverse' Packages (Version 1.1.1). Retrieved from https://cran.r-project.org/web/packages/tidyverse/index.html

Zasko, D. N., & Rusanov, I. I. (2005). Vertical distribution of radiolarians and their role in epipelagic communities of the East Pacific rise and the Gulf of California. *Biology Bulletin*, *32*(3), 279–287. https://doi.org/10.1007/s10525-005-0103-5